Article

Cell Reports

Estrogen Regulates the Satellite Cell Compartment in Females

Graphical Abstract

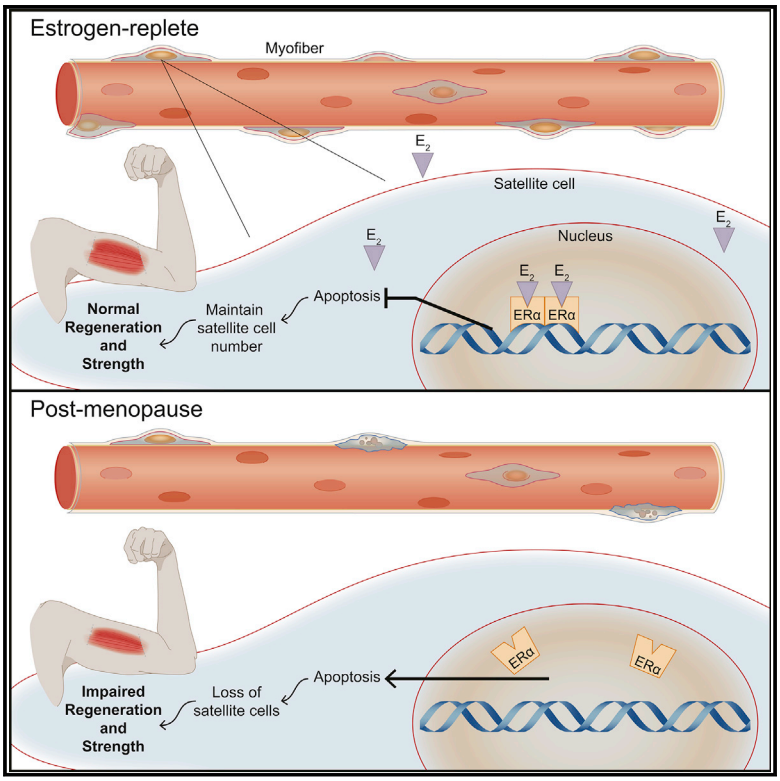

Highlights

- Estrogen sustains the satellite cell number in the muscle of female rodents and humans
- Estrogen signals selectively through ERα in satellite cells
- Loss of ERα in satellite cells provokes apoptosis and satellite cell loss
- Loss of estrogen-ERα signaling impairs muscle strength recovery following injury

Authors

Brittany C. Collins, Robert W. Arpke, Alexie A. Larson, ..., Espen E. Spangenburg, Michael Kyba, Dawn A. Lowe

Correspondence

lowex017@umn.edu

In Brief

Collins et al. show the loss of estrogen in female mice and post-menopausal women leads to a decrease in skeletal muscle stem cells. Using muscle stem cell-specific mutants, it was demonstrated that ERα is necessary for satellite cell maintenance, self-renewal, and protection from apoptosis, thereby promoting optimal muscle regeneration.

Collins et al., 2019, Cell Reports *28*, 368–381
July 9, 2019
https://doi.org/10.1016/j.celrep.2019.06.025

CellPress

OPEN ACCESS
CellPress

Cell Reports
Article

Estrogen Regulates the Satellite Cell Compartment in Females

Brittany C. Collins,[1,6] Robert W. Arpke,[2,7] Alexie A. Larson,[3] Cory W. Baumann,[1] Ning Xie,[2] Christine A. Cabelka,[1] Nardina L. Nash,[1] Hanna-Kaarina Juppi,[4] Eija K. Laakkonen,[4] Sarianna Sipilä,[4] Vuokko Kovanen,[4] Espen E. Spangenburg,[5] Michael Kyba,[2] and Dawn A. Lowe[1,8,*]

[1]Divisions of Rehabilitation Science and Physical Therapy, Department of Rehabilitation Medicine, Medical School, University of Minnesota, Minneapolis, MN, USA
[2]Lillehei Heart Institute and Department of Pediatrics, Medical School, University of Minnesota, Minneapolis, MN, USA
[3]Department of Integrative Biology and Physiology, Medical School, University of Minnesota, Minneapolis, MN, USA
[4]Gerontology Research Center, Faculty of Sport and Health Sciences, University of Jyväskylä, Jyväskylä, Finland
[5]East Carolina Diabetes and Obesity Institute, Department of Physiology, Brody School of Medicine, East Carolina University, Greenville, NC, USA
[6]Present address: Department of Human Genetics, University of Utah, 15 North 2030 East, Salt Lake City, UT 84112, USA
[7]Present address: Division of Biological Sciences, University of Missouri, 105 Tucker Hall, Columbia, MO 65211, USA
[8]Lead Contact
*Correspondence: lowex017@umn.edu
https://doi.org/10.1016/j.celrep.2019.06.025

SUMMARY

Skeletal muscle mass, strength, and regenerative capacity decline with age, with many measures showing a greater deterioration in females around the time estrogen levels decrease at menopause. Here, we show that estrogen deficiency severely compromises the maintenance of muscle stem cells (i.e., satellite cells) as well as impairs self-renewal and differentiation into muscle fibers. Mechanistically, by hormone replacement, use of a selective estrogen-receptor modulator (bazedoxifene), and conditional estrogen receptor knockout, we implicate 17β-estradiol and satellite cell expression of estrogen receptor α and show that estrogen signaling through this receptor is necessary to prevent apoptosis of satellite cells. Early data from a biopsy study of women who transitioned from peri- to post-menopause are consistent with the loss of satellite cells coincident with the decline in estradiol in humans. Together, these results demonstrate an important role for estrogen in satellite cell maintenance and muscle regeneration in females.

INTRODUCTION

Over the course of an individual's life, skeletal muscle undergoes numerous injurious insults that require repairs in order for function to be maintained. The maintenance and injury repair of skeletal muscle is dependent on its resident stem cell (i.e., the satellite cell), with genetic ablation of satellite cells completely abolishing the ability of skeletal muscle to regenerate following injury (Fry et al., 2015; Murphy et al., 2011; Sambasivan et al., 2011). Satellite cells are located between the sarcolemma and the basal lamina of skeletal muscle fibers, where they remain in a quiescent state (Conboy and Rando, 2002; Fukada et al., 2007; Keefe et al., 2015; Kuang et al., 2007), becoming activated through external stimuli, such as a muscle injury, initiating the transition from quiescence into the myogenic program to repair damaged muscle (Conboy and Rando, 2002; Dumont et al., 2015; Hindi and Kumar, 2016; Kuang et al., 2007; Troy et al., 2012). With proliferation, satellite cells undergo asymmetric division through which a subpopulation of the daughter satellite cells do not differentiate, but instead return to quiescence, repopulating the satellite cell pool (i.e., self-renewal) (Kuang et al., 2007; Troy et al., 2012). The balance of this asymmetric division process is critical and necessary to ensure the life-long preservation of satellite cells in skeletal muscle.

Aging diminishes the satellite cell pool (Keefe et al., 2015; Sajko et al., 2004; Verdijk et al., 2014) and, as a result, the regenerative capacity of skeletal muscle in aged males is impaired compared to that of younger males (Brack et al., 2005; Carlson and Conboy, 2007; Chakkalakal et al., 2012; Keefe et al., 2015; Shefer et al., 2006), but such age-induced impairments in females is less studied. Similarly, age-associated changes in the satellite cell environment, in combination with cell-intrinsic alterations, disrupt quiescence and the balance of asymmetric division, ultimately impacting satellite cell maintenance and muscle regenerative potential (Bernet et al., 2014; Conboy et al., 2005; Cosgrove et al., 2014; Sousa-Victor et al., 2014). Such results support the concept that circulatory factors, including hormones that differ between the young and old systemic environments and the activity of their subsequent signaling pathways, contribute to age-associated decrements in satellite cell maintenance and overall muscle regenerative capacity.

A well-known hormone that changes with age is estradiol, the main circulating sex hormone in adult females. Estradiol is not only a major regulator of gonadal organ development and function, but it is also now recognized for its protective effects in other tissues (e.g., against cardiovascular disease and osteoporosis) in women prior to the menopausal transition (Deschamps et al., 2010). Serum estradiol concentration declines dramatically

at the average age of 51 in women, corresponding to the time of menopause (Baber et al., 2016). Estradiol deficiency reduces skeletal muscle mass and force generation in women (Greising et al., 2009; Phillips et al., 1993, 1996; Qaisar et al., 2013; Taaffe et al., 2005) and female rodents (Greising et al., 2011; Moran et al., 2007) and prevents the recovery of strength following contraction-induced muscle injury (Kosir et al., 2015; Rader and Faulkner, 2006) and traumatic muscle injury in female mice (Le et al., 2018). However, evidence that this regenerative phenotype involves effects of estradiol directly on satellite cells is lacking. For example, the estrogen requirement for muscle regeneration has previously been based simply on a lower mass, cross-sectional area, and a fibrosis index of a single muscle at a single time point (14 d) following a single type of injury with no changes in satellite cell number (Kitajima and Ono, 2016). Previous work has also indicated that exercise-induced activation of satellite cells is less effective in the absence of estradiol (Enns and Tiidus, 2008) and that androgens contribute to the regulation of juvenile satellite cells during growth (Kim et al., 2016), but it has yet to be determined if there are cell-autonomous (receptor- or non-receptor-mediated) mechanisms that involve estradiol acting directly on satellite cells.

In this study, we use rigorous and unbiased approaches (e.g., two independent sets of markers to quantify satellite cell numbers from entire muscles by flow cytometry, in five different muscles, at three time points of estrogen deficiency, as well as by an independent method immunohistochemistry, plus reversal of the phenotype by treating mice with estradiol and measurements of self-renewal and differentiation by transplantation) to demonstrate the *in vivo* necessity of estradiol to maintain the satellite cell number in females. Further, we use mouse genetics to show that the molecular mechanism of estradiol action is cell-autonomous signaling through estrogen receptor α (ERα). Specifically, we show the functional consequence of estradiol-ERα ablated signaling in satellite cells including impaired self-renewal, engraftment, and muscle regeneration, and the activation of satellite cell mitochondrial caspase-dependent apoptosis.

RESULTS

Estradiol Regulates Satellite Cell Maintenance

To directly test whether ovarian hormone deficiency affects the satellite cell compartment, we counted the total number of satellite cells in five diverse muscles from control and ovariectomized (Ovx) mice (Figure S1). Satellite cells (lineage negative; vascular cell adhesion protein [VCAM], alpha7 double positive) were 30%–60% fewer in number in tibialis anterior (TA) muscles of Ovx than control mice, and reduction was associated with the duration of hormone deficiency (Figure 1A). Extensor digitorum longus (EDL), gastrocnemius, and diaphragms in Ovx mice had reduced satellite cell numbers as well (Figure 1A). The soleus, which is a slower and more fatigue-resistant muscle, was unaffected by hormone manipulation (Figure 1A). We also evaluated the density of satellite cells, calculated by dividing the cell number (Figure 1A) by the wet mass of each muscle (Figures 1B and 1C). Satellite cell density recapitulated the cell number declines with ovarian hormone deficiency in the TA, gastrocnemius, and EDL muscles. In the diaphragm, where the decline in total number was only statistically significant at the 2-month point, the decline in satellite cell density was statistically significant at all time points studied (Figure 1C).

To confirm the effect of ovarian hormone deficiency on the satellite cell number using an independent marker, we employed the Pax7-ZsGreen mouse model, in which quiescent satellite cells fluoresce green, and differentiating cells rapidly lose fluorescence (Bosnakovski et al., 2008). Consistent with results from surface marker staining, ZsGreen+ cells were significantly lower in the TA, EDL, and gastrocnemius muscles of 2-month hormone-deficient Ovx mice compared to control, with the diaphragm trending and soleus again being less affected (Figure S2). We also counted the Pax7+ cells in immuno-stained TA muscle sections to independently verify the results of fluorescence-activated cell sorting (FACS) quantification (Figure 1D). Histological analysis showed that TA muscles from Ovx mice have ~50% fewer satellite cells than controls (Figure 1E).

Ovariectomy results in systemic changes and deficiencies of multiple hormones. To determine if estradiol was the hormone responsible for affecting satellite cells, a subset of Ovx mice was treated with 17β-estradiol simultaneously with Ovx. Treatment with this specific ovarian hormone rescued satellite cell numbers, preventing depletion of the satellite cell pool (Figures 2A–2D), thus demonstrating sufficiency for the hormone estradiol.

Given that the loss of estradiol perturbs maintenance of the satellite cell pool during homeostatic conditions, we aimed to determine if this loss of satellite cell number resulted in functional consequences. We investigated if recovery of function (i.e., strength) from a chemical injury to the TA muscle was affected by the loss of estradiol (Ovx+Placebo). Following a single bout of injury, estradiol deficiency did not affect strength recovery until 21 days post-injury, which resulted in a 19% lower torque strength ($p = 0.06$; Figure 2E). Strikingly, following a second bout of injury, strength recovery was substantially lower by 23%–39% at the three time points: 28, 35, and 42 days post-injury. Treatment with estradiol (Ovx+E_2) rescued the decrements in strength ($p \leq 0.019$; Figure 2E). These results demonstrate that the decline in satellite cell number is associated with an impaired regenerative response.

Estradiol Deficiency Impairs Self-Renewal and Differentiation *In Vivo*

The disruption of satellite cell maintenance and the impairment in strength recovery following injury that occurred with the loss of estradiol led us to next determine if self-renewal and/or differentiation were affected, as these cellular processes have direct implications for the replenishment of the satellite cell pool. We assayed self-renewal and differentiation *in vivo* via transplantation. Satellite cells were harvested from bulk hindlimb cell preparations from female Pax7-ZsGreen mice, and 600 cells were transplanted into previously irradiated, cardiotoxin-injured TA muscles of control or Ovx recipient syngeneic C57/BL6J mice (Figure 3A). Satellite cell engraftment was measured by FACS using the donor ZsGreen+ marker, which is maintained only in the undifferentiated Pax7+ donor-derived satellite (Figure 3B). Estradiol deficiency of the recipient resulted in 75% lower

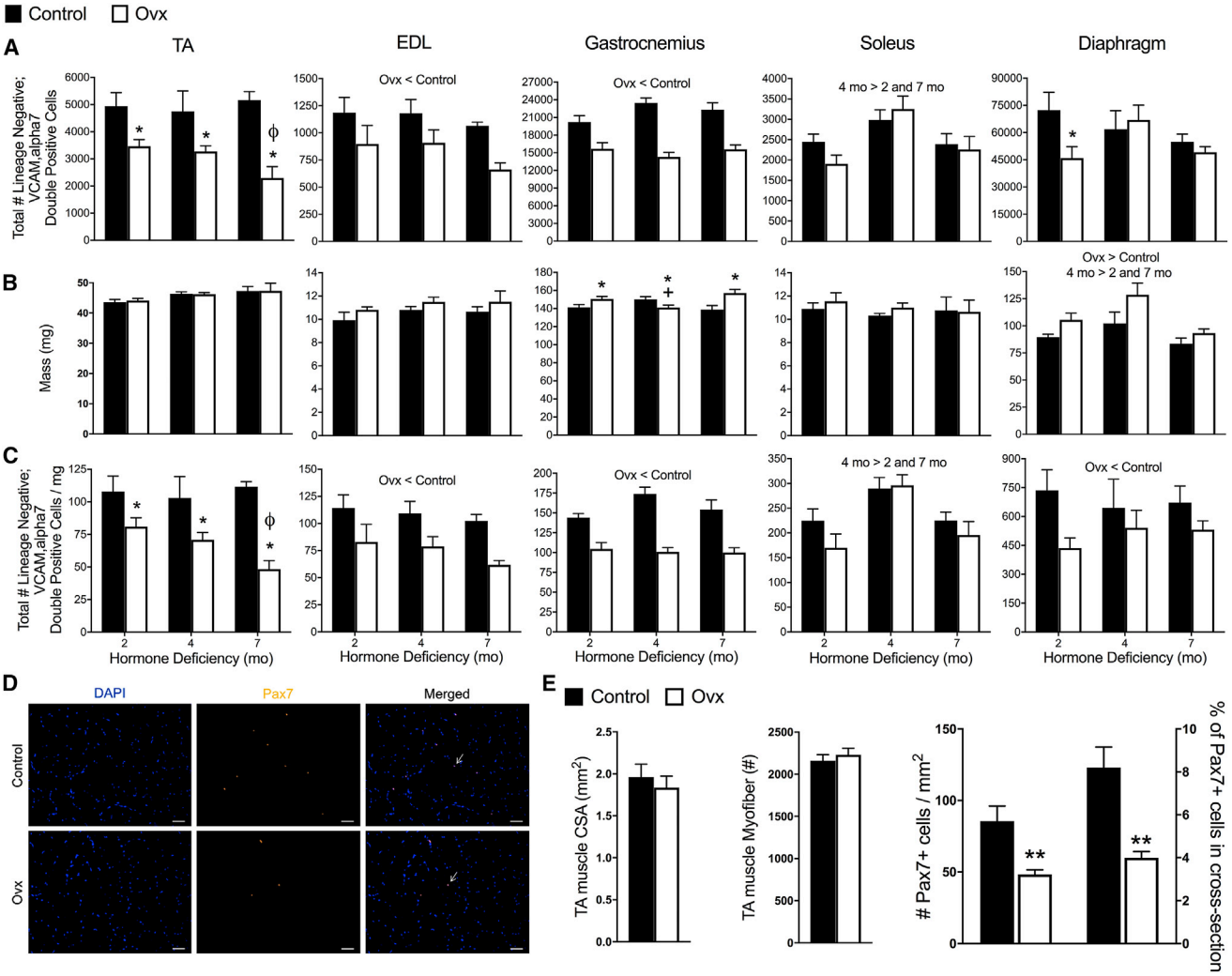

Figure 1. Estrogen Deficiency Disrupts Maintenance of Satellite Cells in Skeletal Muscles of Females

(A) Total number of satellite cells quantified by lineage negative;VCAM,alpha7 double-positive cells in five discrete muscles from control (n = 15) and ovariectomized (Ovx; n = 15) mice. Muscles were harvested and analyzed 2, 4, or 7 months after Ovx and in age-matched controls.

(B) Muscle masses.

(C) Total number of satellite cells normalized to muscle masses.

(D) Satellite cells quantified by immunohistochemistry of Pax7+ cells in TA muscles from control (n = 4) and Ovx (n = 4) mice at 2 months of hormone deficiency. Arrows indicate localization of DAPI+ Pax7+double-positive cell. Scale bars, 50 μm.

(E) TA muscle cross-sectional area and number of fibers from control and Ovx mice ($p \geq 0.193$), and Pax7+ cells per TA muscle cross-sectional area and % Pax7+ cells in each cross section relative to the total number of muscle fibers.

Significant main effects of two-way ANOVA ($p < 0.05$) are indicated above the bars (A–C) and when interactions occurred ($p < 0.05$), Holm-Sidak post hoc tests are indicated by the following symbols: *, different than control at corresponding duration (A–C); ϕ, different than 2- and 4-month Ovx (A and C); and +, different than 2- and 7-month Ovx (B). **$p < 0.005$ by Student's t tests (E).

engraftment of the satellite cell compartment compared to control recipients (Figure 3C).

To address the contribution of satellite cells to fibers, we utilized a lineage-tracing strategy (*Pax7* $^{CreERT2/+}$; *R26R*^{tdTom} mice) to mark donor-derived fibers (Figure 3D). This experiment again confirmed the deleterious effect of systemic estradiol deficiency on satellite cell engraftment (Figures 3E and 3F) and further demonstrated that while satellite cells contributed robustly to fibers in the muscle of control recipients, contribution to fibers was minimal when estradiol was not present (Figures 3G and 3H). As a result of the reduced engraftment and differentiation potential of the satellite cells when transplanted from an estradiol-replete environment into one lacking estradiol, we next aimed to determine if satellite cells from an environment lacking estradiol (i.e., from Ovx donors) were intrinsically, irreversibly impaired, or whether they would be functional in an estrogen-replete environment. ZsGreen+ satellite cells were isolated from the TA and gastrocnemius muscles of control and Ovx

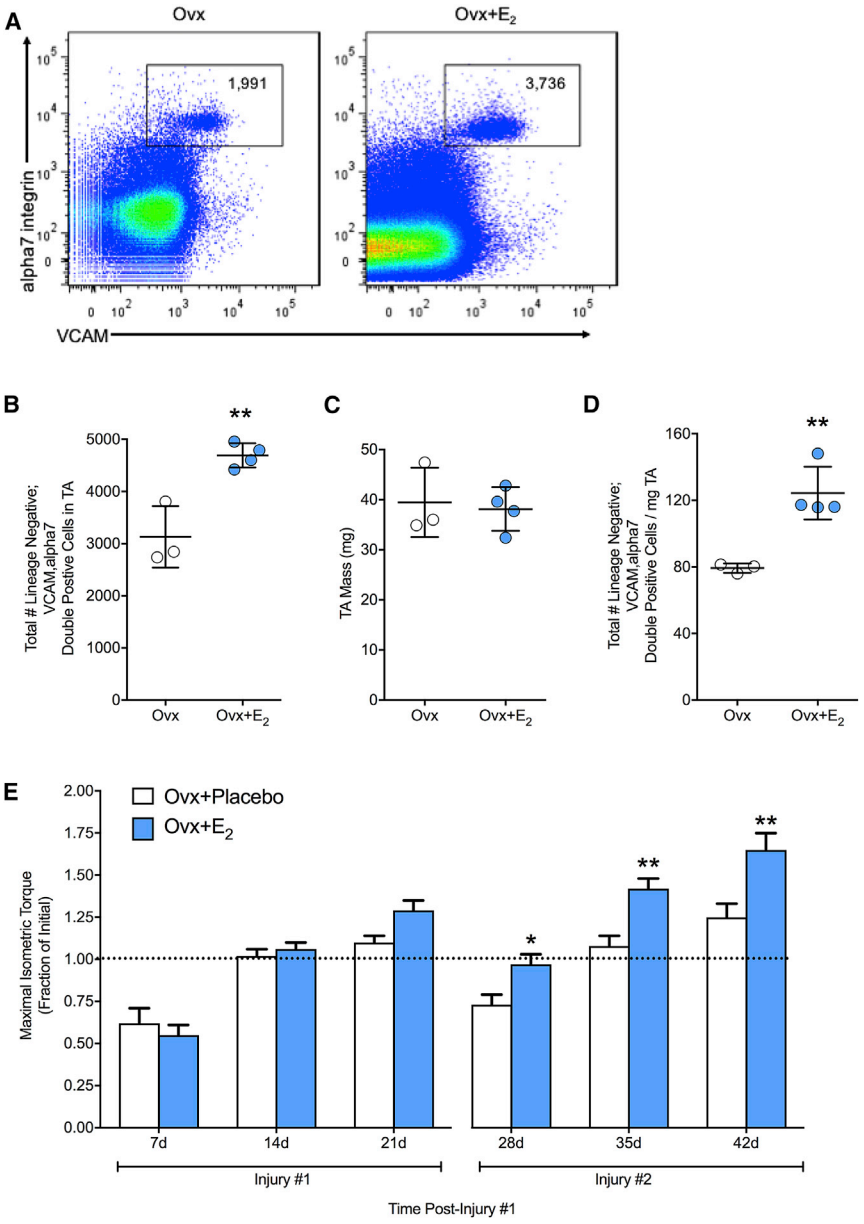

Figure 2. Estradiol Maintains the Satellite Cell Pool and Accelerates Recovery of Strength

(A) Representative FACS plots of cells isolated from TA muscles of Ovx mice without (n = 3) and with 17β-estradiol treatment (Ovx+E_2; n = 4).

(B) Total number of satellite cells.

(C) TA muscle mass.

(D) Total number of satellite cells relative to TA muscle mass.

(E) Maximal isometric torque (i.e., strength) expressed relative to pre-injury torque in Ovx mice without (Ovx+Placebo; n = 6) or with 17β-estradiol treatment (Ovx+E_2; n = 8) following repeated injuries to TA muscle.

*p < 0.05 and **p < 0.005 by Student's t tests (A–D) and Holm-Sidak post hoc (E).

donor mice, and 600 cells were transplanted into control recipients (Figure 3I). The transfer into an estradiol-replete environment (i.e., control recipient) rendered satellite cells from Ovx mice similar to those of controls (Figures 3J and 3K).

In Humans, Satellite Cell Number Declines during the Menopausal Transition

Satellite cell number declines with age in humans; however, the majority of studies have compared muscle from old men (~70 year old) to young men (~20 year old), and the studies have been cross-sectional in design (Verdijk et al., 2012, 2014). To date, satellite cell number has not been evaluated during the menopausal transition in women, nor to our knowledge have any aging longitudinal studies of satellite cell numbers been conducted in humans. Here, we aimed to determine if the satellite cell number declines during the peri- to post- menopausal transition in women by taking two muscle biopsies from the same women at peri- and post-menopause and staining these for Pax7 (Figures 4A and 4B). Satellite cell number declined 15% on average during the transition and trended very close to statistical significance (p = 0.057; Figure 4C), and declines were observed in four out of the five women (Figure 4D). This reduction is striking since the peri- to post-menopause transition in these women occurred within a 1-year time period, and the cell number declines cannot be attributed to reduced physical activity or myofiber size (Figure 4A). We observed that not all study participants displayed the same degree of estradiol loss across the time in which longitudinal biopsies were obtained. Thus, we performed a Pearson correlation between serum concentration of estradiol and satellite cells in peri- and post-menopausal samples from the same five women (Figure 4E). The result is a strong correlation that met statistical significance (r^2 = 0.478 p = 0.023; Figure 4F), indicating that even with the low sample size not yet allowing the acceptance of the hypothesis of a sudden satellite cell decline at the peri-to-post-menopausal transition, the data support that changes in the satellite cell number across this transition are related to changes in 17β-estradiol concentration.

ERα Is the Relevant ER in Satellite Cells

There are three known ERs in skeletal muscle: ERα, ER beta (ERβ), and g-protein coupled ER (GPER). We have recently established that the effects of estradiol on force generation by skeletal muscle are mediated by ERα (Collins et al., 2018). This result, in combination with other work showing ERα is involved

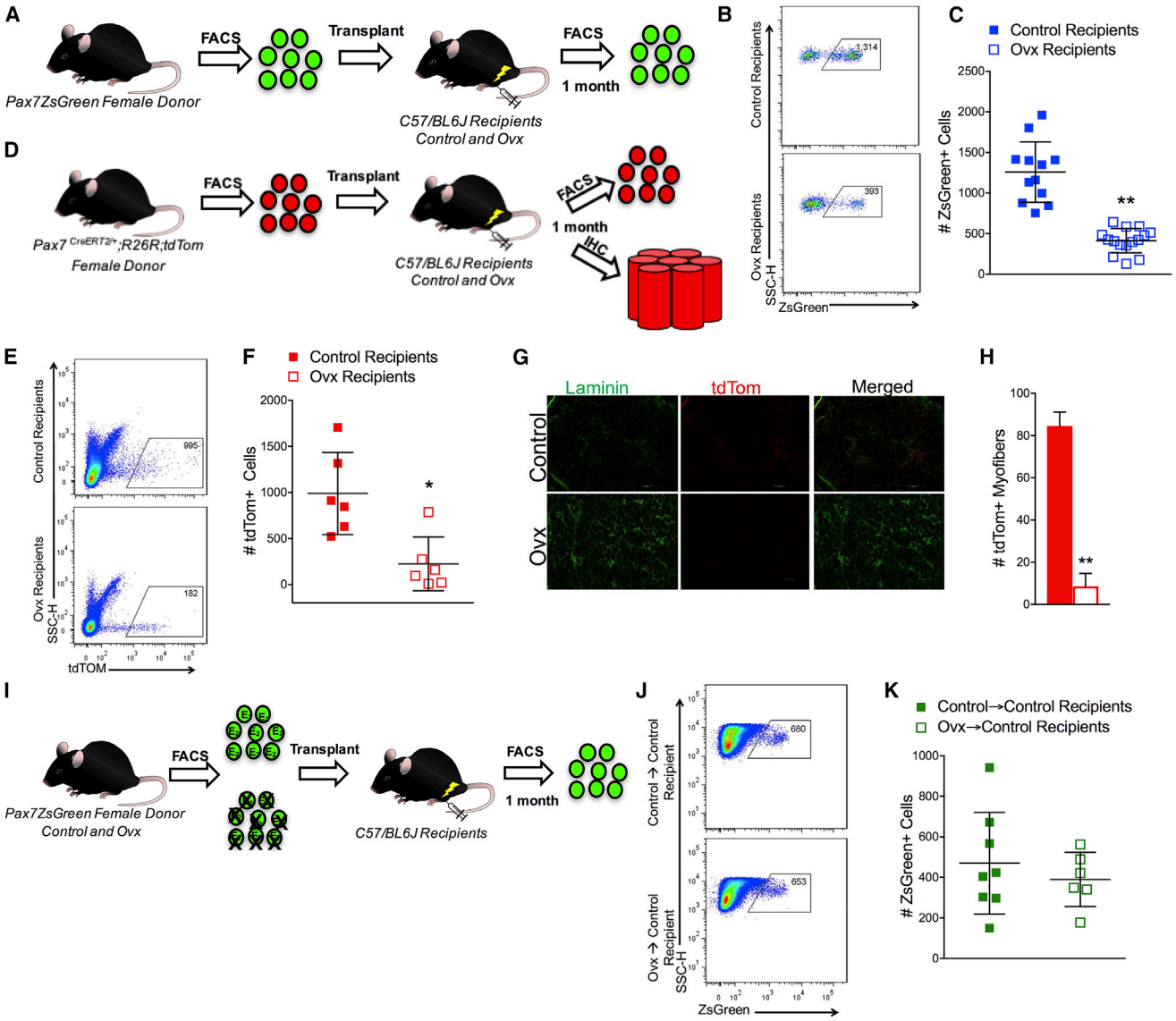

Figure 3. Loss of Estradiol in the Environment Negatively Affects Satellite Cell and Fiber Engraftment That Can be Rescued by the Presence of Estradiol

(A) Transplantation scheme for ZsGreen+ cells transplanted into control and Ovx recipients.

(B) Representative FACS plots of ZsGreen+ donor satellite cells in TA muscle 1 month post-transplant in control and Ovx recipient mice.

(C) Total number of ZsGreen+ donor satellite cells in control (n = 12) and Ovx (n = 15) recipient mice 1 month post-transplant.

(D) Scheme for tdTom+ cells transplanted into control (n = 6) and Ovx (n = 6) recipients.

(E) Representative FACS plots of tdTomato red fluorescent protein (tdTOM)+ donor satellite cells in TA muscle 1 month post-transplant in control and Ovx recipient mice.

(F) Total number of tdTOM+ donor satellite cells in control (n = 6) and Ovx (n = 6) recipient mice 1 month post-transplant.

(G) Representative images of tdTom+ fibers in the engrafted region of TA muscle from control and Ovx recipient mice. Scale bars, 100 μm.

(H) Quantification of total number of tdTom+ fibers from control and Ovx recipients.

(I) Transplantation scheme for ZsGreen+ cells from control and Ovx donors.

(J) Representative FACS plots of ZsGreen+ control and Ovx donor satellite cells in TA muscle 1 month following transplant in control recipient mice.

(K) Total number of ZsGreen+ control (n = 8) and Ovx (n = 6) donor satellite cells in control recipient TA muscles 1 month post-transplantation.

*$p < 0.05$ and **$p < 0.005$ by Student's t tests.

in regulating muscle metabolism (Hamilton et al., 2016; Ribas et al., 2016; Ronda et al., 2013) and oxidative stress (Baltgalvis et al., 2010; Vasconsuelo et al., 2008), led us to determine the following: (1) whether satellite cells express female sex hormone receptors; (2) which ER is most highly expressed in satellite cells; and (3) whether this receptor was essential in mediating the

A

	Perimenopausal	Postmenopausal	P-value
Age (yr)	52.9 (0.8)	53.8 (0.9)	0.043
17β-Estradiol (nM)	0.235 (0.04)	0.172 (0.03)	0.042
Follicle-Stimulating Hormone (IU/L)	42.7 (4.2)	66.7 (10.7	0.043
Moderate-to-Vigorous Physical Activity (min/d)	38.6 (10.2)	53.6 (14.1)	0.043
Body Fat (%)	34.8 (2.6)	37.5 (3.6)	0.080
Fat Free Mass (kg)	46.8 (1.1)	45.7 (1.1)	0.080
Total Myofibers Counted (#)	560 (121)	721 (301)	0.500
Myofiber CSA (μm²)	3099 (306)	3092 (252)	0.686

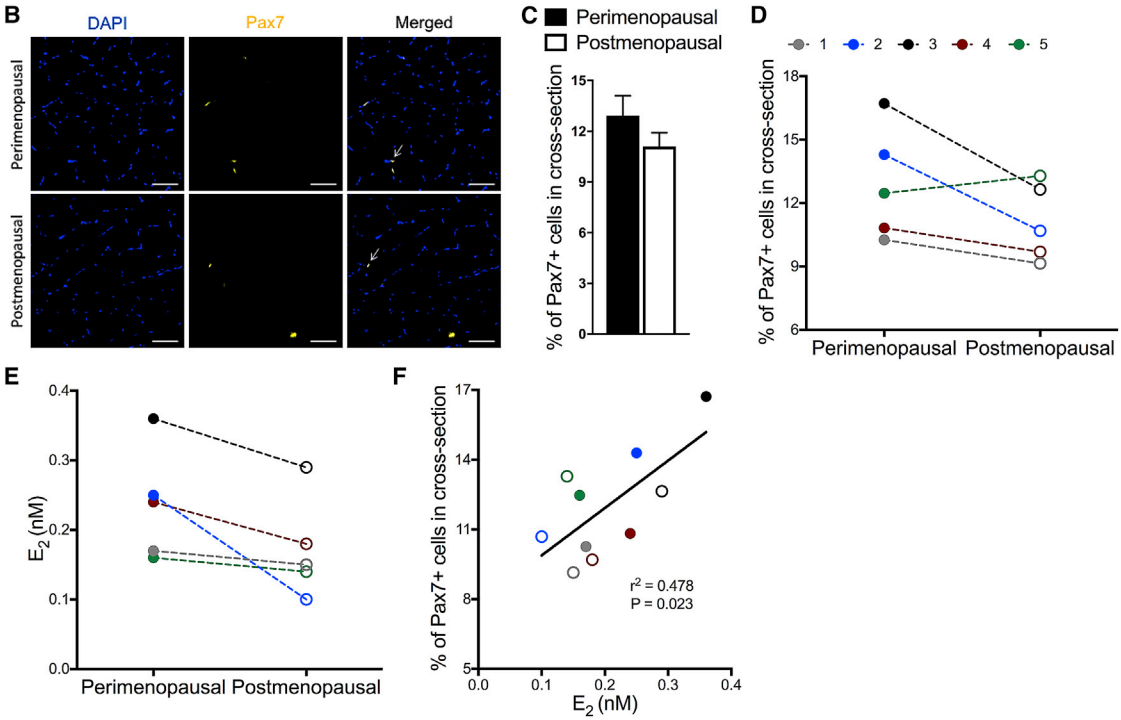

Figure 4. Peri- to Post-Menopausal Transition Results in Decline of Muscle Satellite Cells in Humans

(A) Subject characteristics of women participants (n = 5).

(B) Representative images of DAPI stained nuclei (blue), Pax7 satellite cells (gold), and merged images from cross sections of muscle biopsies from peri-menopausal women and of the same women when post-menopausal status was reached. Scale bars, 50 μm.

(C) Quantification of percentage of Pax7+ cells counted in each cross section relative to the total number of fibers in muscle biopsies from peri-menopausal and post-menopausal women (p = 0.057).

(D) Declines in the percentage of Pax7+ cells in muscle cross sections of four out of five individual women during the two menopausal stages.

(E) Individual serum estradiol (E_2) levels in women during the two menopausal stages.

(F) Pearson correlation between E_2 and %Pax7+ cells (p = 0.023). Peri-menopausal women shown in closed circles and post-menopausal women shown in open circles (def).

activity of estradiol on satellite cell function. RNA sequencing (RNA-seq) and qRT-PCR on sorted Pax7-ZsGreen+ cells (Figure 5A) showed that satellite cells express *Esr1*, the gene encoding ERα, significantly more than the other two ERs, *Esr2* (ERβ) and *Gper1*, and the progesterone receptor, *Pgr* (Figure 5B). To this point, *Esr2*, *Gper1*, and *Pgr* had transcript per kilobase million (TPM) expression values less than 1 (Figure 5B), and *Esr2* was undetectable in our qRT-PCR analysis. *Esr1* was also more highly expressed in ZsGreen+ cells compared to other mononuclear cells (ZsGreen− cells) (Figure 5C). Therefore, we developed an inducible satellite cell-specific ERα knockout model (Figures 5D–5F) in order to specifically probe the necessity of ERα in the mechanism by which estradiol mediates effects on satellite cells. The genetic deletion of ERα did not result in the compensation of the other hormone receptors in satellite cells (Figures 5D–5F).

Estradiol Signals Cell Autonomously to Maintain Satellite Cell Number

We treated *Pax7*$^{CreERT2/+}$; *Esr1*$^{fl/fl}$;*Pax7-ZsGreen* female mice (scERαKO) and *Pax7*$^{+/+}$;*Esr1*$^{fl/fl}$;*Pax7-ZsGreen* control sibling females (scERαWT) with tamoxifen to ablate ERα and evaluate satellite cell frequency in multiple muscle groups by FACS (Figure S3). Ablation of ERα in satellite cells resulted in 40%–60% fewer satellite cells in all five muscles analyzed; again, both expressed in terms of absolute cell numbers and satellite cell

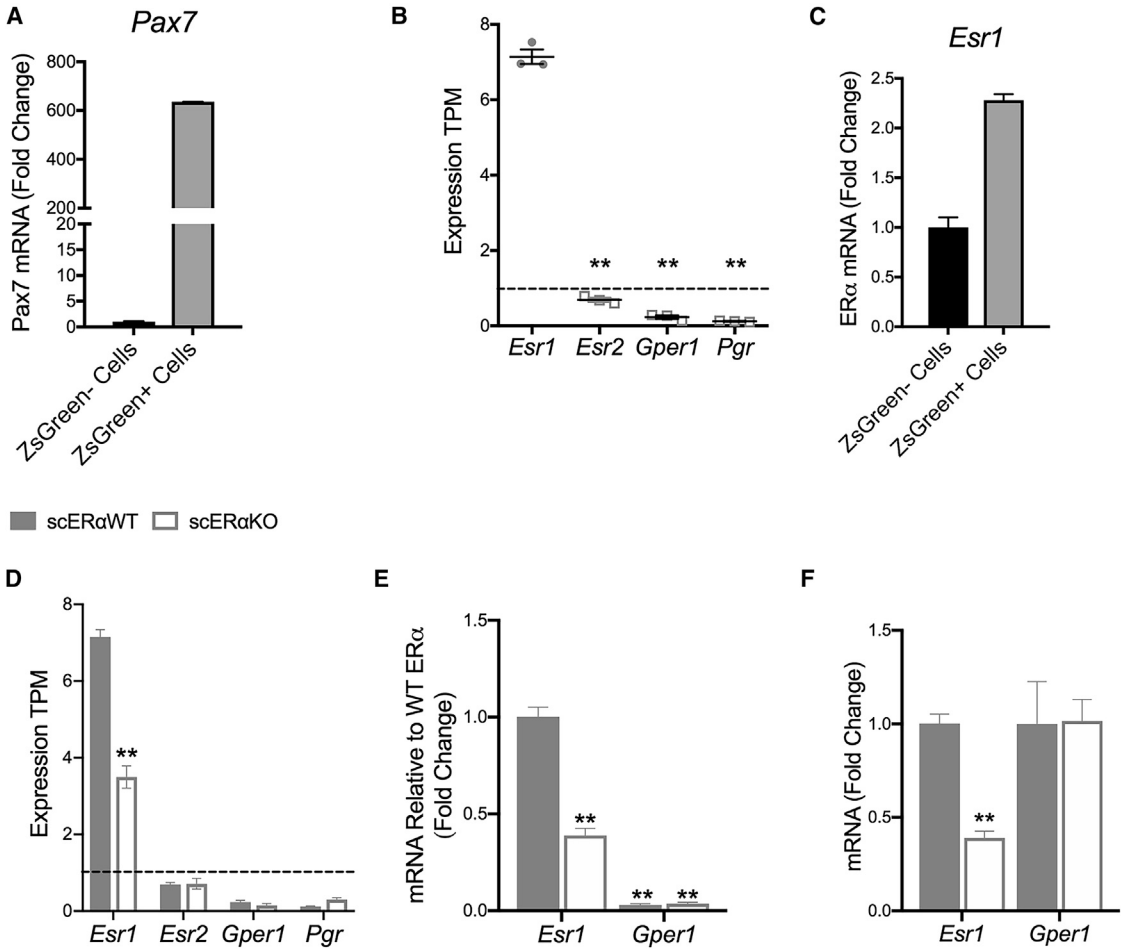

Figure 5. Estrogen Receptor Alpha (ERα) Is the Relevant Hormone Receptor in Satellite Cells

(A) mRNA gene expression of *Pax7* in isolated ZsGreen+ satellite cells from Pax7-ZsGreen female mice (n = 4).

(B) Transcripts per kilobase million (TPM) of ER alpha (*Esr1*), ER beta (*Esr2*), g-protein coupled ER (*Gper1*), and progesterone receptor (*Pgr*) in isolated ZsGreen+ satellite cells from Pax7-ZsGreen mice (n = 3).

(C) mRNA gene expression of *Esr1* ZsGreen− mononuclear cells and Zsgreen+ satellite cells from Pax7-ZsGreen mice (n = 4)

(D) TPM of *Esr1*, *Esr2*, *Gper1*, and *Pgr* in $Pax7^{+/+}$;$Esr1^{fl/fl}$;*Pax7-ZsGreen* (scERαWT; n = 3) and $Pax7^{CreERT2/+}$;$Esr1^{fl/fl}$;*Pax7-ZsGreen* (scERαKO; n = 3) mice.

(E and F) mRNA gene expression of *Esr1* and *Gper1* (E) relative to *Esr1* expression and (F) relative to that in scERαWT in isolated ZsGreen+ satellite cells from scERαWT (n = 3) and scERαKO (n = 4) mice.

ANOVA, Holm-Sidak post hoc tests indicated by **p < 0.005, significantly different from *Esr1* (B) or scERαWT (D–F)

density (i.e., normalized to muscle mass) (Figures 6A–6C). We replicated these results by performing Pax7 immuno-staining of TA muscle cross sections from scERαWT and scERαKO female mice (Figure S3). The magnitude of the satellite cell reductions was similar to those of the estradiol deficiency (compare Figures 6A–6C with Figures 1A–1C). Furthermore, the removal of ovarian hormones (scERαKO+Ovx) and the treatment of estradiol (scERαKO+Ovx+E_2) in scERαKO mice did not result in a further decline or a rescue of the satellite cell number, respectively (Figures 6D–6F). These results mechanistically show that ERα is required for estradiol signaling to maintain the satellite cell pool in muscles of females.

It was not known whether the new selective ER modulator, bazedoxifine (BZA), would be an ER agonist or antagonist in skeletal muscle. We show that Ovx mice treated with BZA rescued the detrimental effects on satellite cell number (p = 0.055; Figure 6G), demonstrating that it is an agonist in muscle. Because BZA functions by binding ERs, this result further supports the concept that estradiol's mechanism of action in satellite cells is receptor mediated.

ERα Is Necessary for Satellite Cell Self-Renewal

We next tested whether the loss of ERα in satellite cells would impair self-renewal using the *in vivo* transplantation assay, similar to what was measured with estradiol deficiency (Figure 6H). 600 ZsGreen+ satellite cells from female scERαWT and scERαKO mice were transplanted into control C57/BL6J recipient mice, and the contribution to the satellite cell compartment was measured by FACS analysis of total recipient muscle 1 month post-transplant (Figures 6H and 6I). Analogous to the Ovx study,

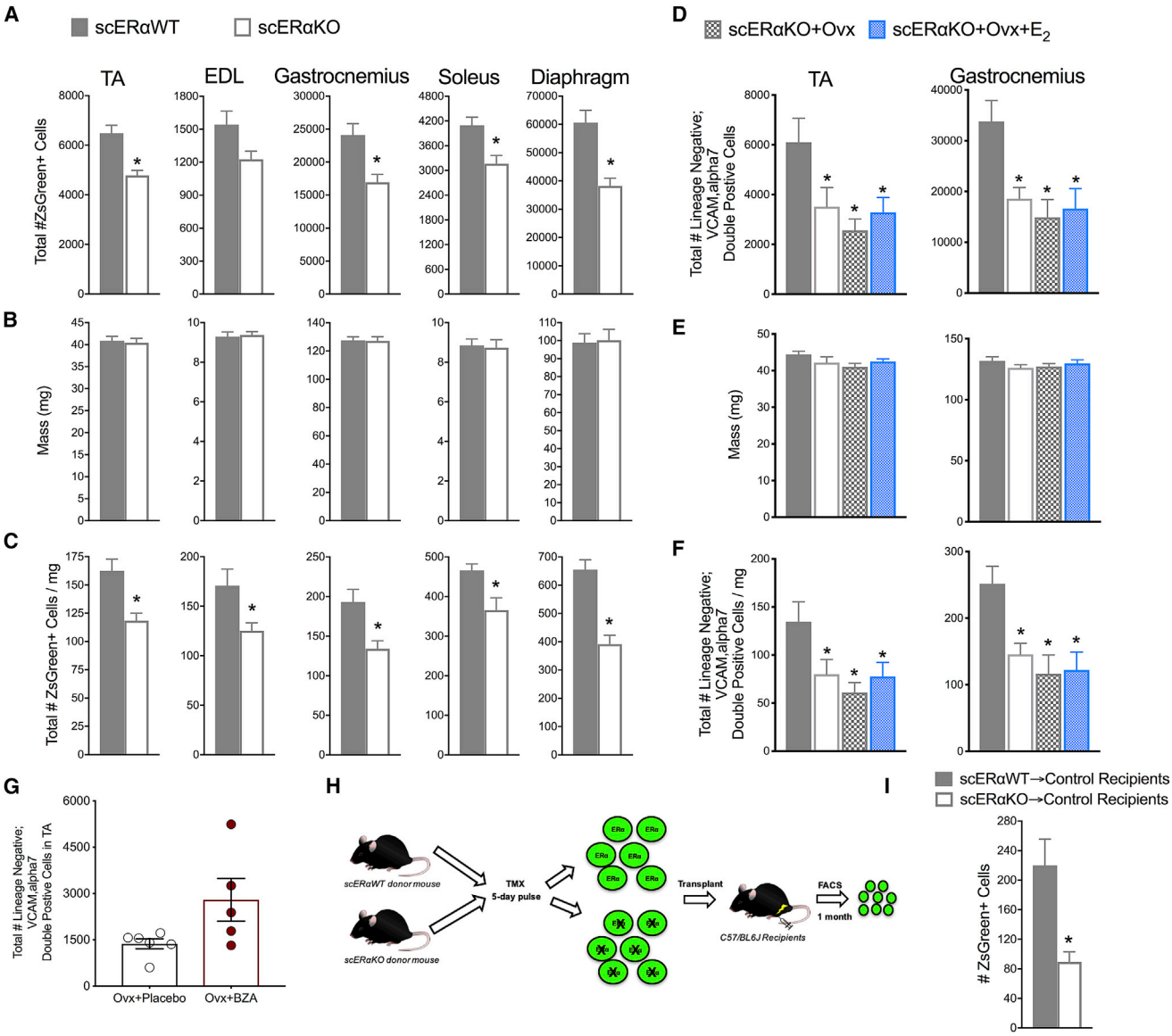

Figure 6. Estradiol Regulates Satellite Cell Number Cell Autonomously through ERα

(A) Total number of ZsGreen+ satellite cells in five muscles of *Pax7*$^{+/+}$;*Esr1*$^{fl/fl}$;*Pax7-ZsGreen* (scERαWT; n = 6) and *Pax7*$^{CreERT2/+}$;*Esr1*$^{fl/fl}$;*Pax7-ZsGreen* (scERαKO; n = 6) mice.

(B) Muscle masses.

(C) Total number of ZsGreen+ cells normalized to muscle mass.

(D) Total number of satellite cells quantified by lineage negative;VCAM,alpha7 double-positive cells in two muscles of scERαWT (n = 6), scERαKO (n = 4), scERαKO+Ovx (n = 5), and scERαKO+Ovx+17β-estradiol (scERαKO+Ovx+E_2; n = 5).

(E) Muscle masses.

(F) Total number of satellite cells normalized to muscle masses.

(G) Total number of satellite cells isolated from TA muscles of Ovx mice without (n = 6) and with Bazedoxifine (Ovx+BZA; n = 5) treatment (p = 0.055).

(H) scERαWT and scERαKO transplantation scheme.

(I) Quantification of ZsGreen+ donor satellite cells in control recipient TA muscles following transplantation.

*p < 0.05 by Student's t tests (A–C, G, and I) *p < 0.05 ANOVA, Holm-Sidak post hoc tests are indicated by *, different from scERαWT (D–F)

we observed a dramatic reduction in satellite cell engraftment in the absence of ERα in donor satellite cells (Figure 6I), supporting the interpretation that ERα is the relevant ER maintaining homeostatic control of self-renewal in response to estradiol.

Apoptosis of Satellite Cells with Estradiol Deficiency

We next investigated whether the mechanism for the reduction in the cell number and impaired self-renewal could involve apoptosis. In non-skeletal muscle tissues, estradiol is known to

protect against apoptosis (e.g., Guo et al., 2013; Zhou et al., 2018), and immortalized myoblasts were also found to undergo less apoptosis *in vitro* in the presence of estradiol (Boland et al., 2008; La Colla et al., 2017; Vasconsuelo et al., 2010). It has been suggested that apoptosis plays an important role in skeletal muscle health, ultimately affecting strength (La Colla et al., 2015; Pallafacchina et al., 2013; Sanchez et al., 2014). However, it is important to point out that in healthy unperturbed muscle, apoptotic cells are from other lineages, and rates of apoptosis of quiescent satellite cells during homeostatic conditions are nearly zero (Fry et al., 2016; Hirai et al., 2010; Shea et al., 2010). First, we measured overall apoptosis *in vivo* by identifying terminal deoxynucleotidyl transferase (TdT) dUTP nick-end labeling (TUNEL)+ cells in the TA muscles of control, Ovx, and Ovx+E_2 mice (Figures S4A and S4B). Muscle from all groups of mice contained apoptotic cells, with estradiol-deficient muscles having 3.7-fold more TUNEL+ cells compared to controls. (Figure S4B). Furthermore, estradiol treatment (Ovx+E_2) was able to rescue this detrimental effect by protecting cells from apoptosis (Figure S4B).

To determine whether any of these newly induced apoptotic cells were actually satellite cells, we counterstained samples with Pax7. Loss of estradiol resulted in 2% of the Pax7 population being apoptotic (i.e., Pax7+TUNEL+ cells), while in controls and estradiol treated, the frequency was close to zero (0.03% and 0.0%, respectively; Figure 7A). To validate these results from the level of transcription, we then isolated Pax7-ZsGreen+ cells from control and Ovx mice and evaluated the transcription of apoptosis-related genes. Estradiol deficiency resulted in 3- to 1500-fold upregulation of *p53*, *p38*, *Becn1*, and *Casp3* gene expression (Figure 7B).

To investigate more deeply the mechanism by which estradiol signaling through ERα maintains satellite cell number and facilitates self-renewal, we performed RNA-seq and compared the transcriptome of ZsGreen+ satellite cells from female scERαWT and scERαKO mice (Figure S4C). Globally, principal component analysis (PCA) revealed patterns of genes that are changed with the loss of ERα (Figure 7C) with TPM >5 and 388 genes being differentially expressed between scERαWT and scERαKO satellite cells (Figure 7D). This was corroborated by the downregulation of classical ERα target genes (Figure 7E). To explore the pathways that were cell-autonomously regulated by ERα, we performed ingenuity pathway analysis (IPA) (Figure S4D), with the top pathway of this analysis being cell death and survival (Figures 7F and S4D). Compared to scERαWT, scERαKO satellite cells exhibited upregulation of genes promoting cell death (e.g., *H19*, *Fndc1*, and *mir378c*) and downregulation of genes promoting cell survival (e.g., *Dhcr24*, *Snord65*, and *mir485*; Figure 7G). To validate this result, we completed qRT-PCR on top hits in the IPA in addition to top apoptotic-related hits in the 388 differentially expressed gene analysis (Figure 7H). To summarize, estradiol and ERα promote satellite cell survival via downregulation of genes associated with mitochondrial caspase-induced apoptosis.

DISCUSSION

The notion that age-associated deficits in skeletal muscle can be driven by extrinsic factors that differ between young and aged environments is well established by heterochronic parabiosis experiments (Brack et al., 2007; Conboy et al., 2005). Estradiol is a particularly interesting hormone in this regard, as its levels are much higher in females than in males (Nelson and Bulun, 2001); levels fall precipitously in females at the menopausal transition (Baber et al., 2016), and hormone therapy has been found to have beneficial effects on skeletal muscle health in postmenopausal women (Phillips et al., 1993; Qaisar et al., 2013). To date, actions of estradiol on skeletal muscle have focused primarily on protein synthesis (Kamanga-Sollo et al., 2010; Toth et al., 2001), inflammation (Le et al., 2018; McClung et al., 2007; Ribas et al., 2010), and force generation (Collins et al., 2018; Lai et al., 2016; Moran et al., 2007). The results presented here show that estradiol is necessary for satellite cell maintenance and function in females. When estradiol is lacking in the systemic environment, the number of satellite cells is reduced by 30%–50% in four of five skeletal muscles studied. This result is in contrast to previous studies that did not detect a loss of satellite cell number with estrogen deficiency (Enns et al., 2008; Kitajima et al., 2015; Kitajima and Ono, 2016; Thomas et al., 2010), perhaps due to less-sensitive approaches than what was used here. Further, we show that the consequence of the estradiol-deficient mediated loss of satellite cells is blunted recovery of strength following injury. Strength recovery from injury is exacerbated by a second bout of injury, suggesting that satellite cell self-renewal or differentiation is impaired.

To this point, satellite cells harvested from an estradiol-rich environment failed to populate the satellite cell compartment when transplanted into a host environment that lacked estradiol, but when satellite cells from the pool remaining in a hormone-deficient environment were transplanted into a host environment with estradiol, engraftment, self-renewal, and differentiation were robust. Moreover, we measured a similar decline in satellite cell pool size when ERα was deleted, specifically from satellite cells in steady-state muscle regardless of whether or not estradiol was in the environment. These results strongly suggest a cell-autonomous role for estradiol signaling through a receptor-mediated mechanism via ERα in the satellite cell itself, the impairment of which leads to a reduction in satellite cell pool size.

In principal, a reduction in stem cell pool size can be explained by three possible mechanisms: differentiation, death, or emigration of cells from the tissue. We find no evidence of increased differentiation in the estradiol-deficient environment. Rather, the opposite appears to hold: when lineage-marked cells were transplanted, there was a greater contribution to differentiated muscle fibers in the estradiol-replete environment than in the deficient environment. Given that an impairment in differentiation would tend to increase the number of stem cells, not decrease it, we feel that the lack of contribution to differentiated muscle in this assay is not due to a differentiation blockade. Rather, because we find a subpopulation of Pax7+ cells that are TUNEL+, together with a very strong apoptotic transcriptional response, it is most likely that Pax7+ cells are being lost to apoptosis. Estradiol is known for anti-apoptotic effects in some other contexts: for example, studies on C2C12 cells provide evidence that estradiol can be protective from H_2O_2-induced apoptosis through modulating P53 and forkhead box transcription factor class O (FOXO) transcription factors and

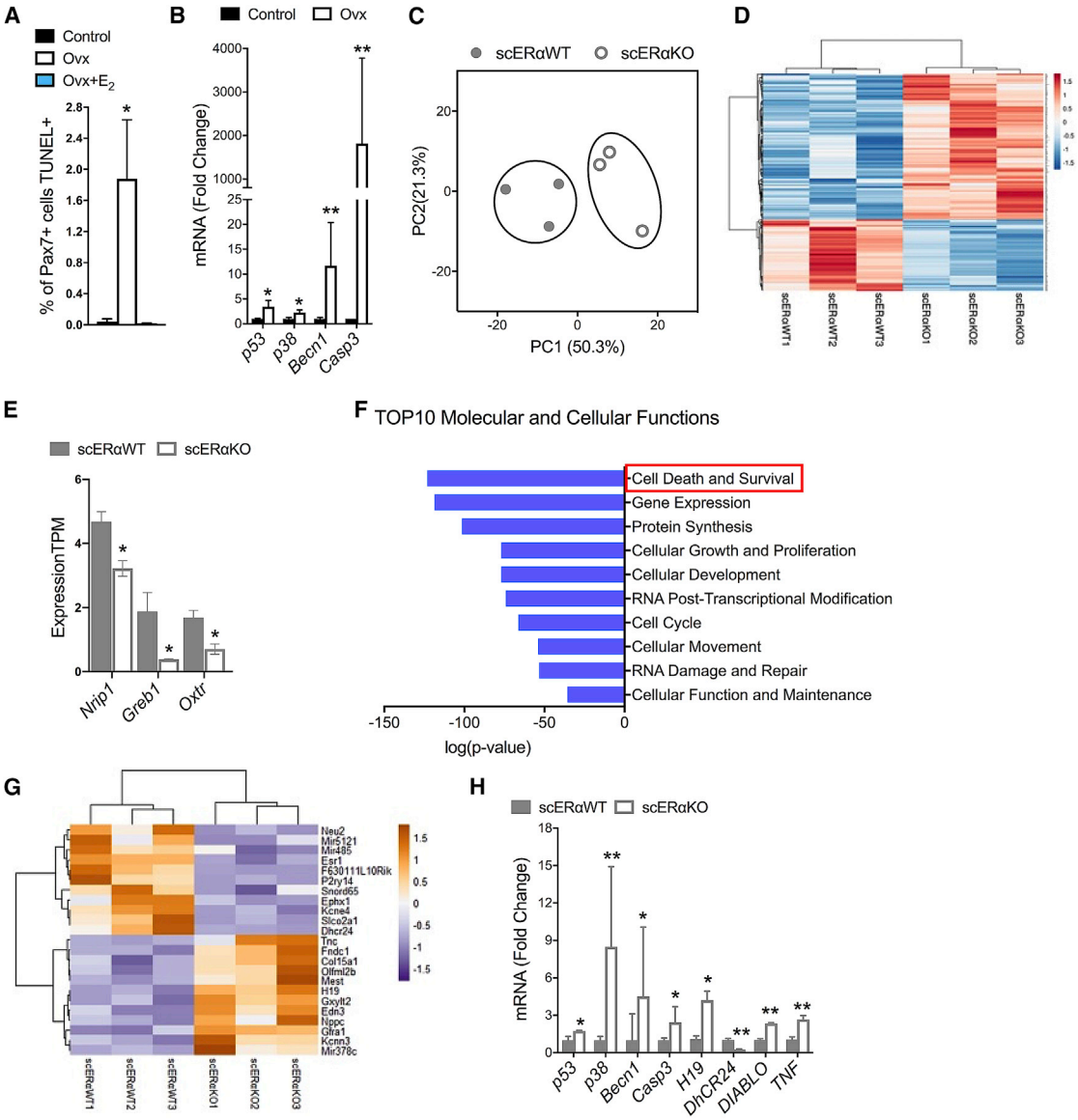

Figure 7. Loss of ERα Results in Satellite Cell Apoptosis

(A) Percent of Pax7+ cells that were also TUNEL+ in cross sections of TA muscles from control (n = 4) and Ovx without (Ovx; n = 4) and with 17β-estradiol treatment (Ovx+E_2; n = 3).

(B) qRT-PCR mRNA expression of apoptosis-related genes in ZsGreen+ satellite cells isolated from gastrocnemius muscles of control (n = 4) and Ovx mice (n = 4).

(C) Principal component analysis (PCA) of RNA-seq profiles of ZsGreen+ satellite cells of *Pax7*$^{+/+}$;*Esr1*$^{fl/fl}$;*Pax7-ZsGreen* (scERαWT; n = 3) and *Pax7*$^{CreERT2/+}$;*Esr1*$^{fl/fl}$;*Pax7-ZsGreen* (scERαKO; n = 3) mice.

(D) Heatmap of 388 differentially expressed genes in satellite cells of scERαWT and scERαKO mice.

(E) Transcripts per kilobase million (TPM) of ERα target genes, nuclear receptor interaction protein (*Nrip*), growth regulating ER binding 1 (*Greb1*), and oxytocin receptor (*Oxtr*).

(F) Top 10 molecular and cellular functions from ingenuity pathway analysis (IPA). Red box to highlight the top pathway, cell death, and survival.

(G) Top 10 upregulated and top 10 downregulated apoptosis-related genes from IPA in satellite cells of scERαWT and scERαKO mice.

(H) qRT-PCR mRNA expression of apoptosis-related genes in ZsGreen+ satellite cells of scERαWT and scERαKO mice.

Significance tested with ANOVA, Holm–Sidak post hoc tests are indicated by *, different from control and Ovx+E_2, *$p < 0.05$ (A) and *$p < 0.05$ and **$p < 0.005$ by Student's t tests (B, E, and G).

their downstream target genes (Boland et al., 2008; La Colla et al., 2017). In pancreatic cells, estradiol is known to signal through a receptor-mediated mechanism to protect against mitochondrial-induced apoptosis (Zhou et al., 2018). Concerning the third possibility, although our studies do not formally rule out emigration of satellite cells from estradiol-deficient muscle, the

scenario seems unlikely because satellite cells do not repopulate via the circulation into muscles that have been completely depleted by freeze injury (although they can migrate into adjacent muscles if connective tissues are disrupted; Schultz et al., 1986).

Hormone therapy is controversial because of the small but detectable increase in breast cancer risk (Kim et al., 2018). The etiology of this disease is thought to be related to estradiol stimulation or mutations in the gene ERα (Dall et al., 2018; Gelsomino et al., 2018; Severson et al., 2018), which is known to exert proliferation of the normal breast tissue (Dall et al., 2018). However, pharmacological progress has been made, and there now exists US Food and Drug Administration (FDA)-approved selective ER modulators (SERMs) (Börjesson et al., 2016). Because SERMs function by inducing conformational changes in ER resulting in tissue-specific agonistic or antagonistic effects, largely depending on which cofactors are present, it was not clear whether the SERM, BZA, would present as an agonist or antagonist in skeletal muscle (Beck et al., 2015; Börjesson et al., 2016). Our results suggest that BZA is an ER agonist in skeletal muscle, or at least in muscle stem cells, as it restored the satellite cell pool in estradiol-deficient mice. This result, along with our finding that ERα is the relevant receptor whose signaling is necessary to maintain the satellite cell pool, supports the use of ERα-selective ligands for therapeutic application in menopause-associated muscle loss.

Notably, we also present preliminary data from a longitudinal biopsy study of aging skeletal muscle. This study tracks muscle in women and employs variable biopsy dates. The first biopsy is at peri-menopause, and the second is at post-menopause, with timing being unique to each participant and determined by changes in their estradiol and follicle stimulating hormone levels. The time between the first and second biopsies was short (~1 year). Accordingly, although we observed a reduction in the mean satellite cell number from the first biopsy to the second, we observed a much greater significance in the correlative analysis between changes in estradiol levels with satellite numbers; this comparison is actually the most relevant to the current study.

In summary, our results demonstrate that estradiol is a necessary factor regulating *in vivo* satellite cell function in female rodents and is supported by similar results in humans. The estradiol-ERα axis contains potential therapeutic targets to mitigate skeletal muscle deficits observed with aging in women. Our study provides a scientific basis for future studies to examine ER agonists, such as BZA, more thoroughly to probe for additional benefits toward overall musculoskeletal health in postmenopausal women. Finally, these collective results highlight the importance of considering biological sex and sex hormones when studying skeletal muscle, particularly regarding age-related deficits in muscle.

STAR★METHODS

Detailed methods are provided in the online version of this paper and include the following:

- KEY RESOURCES TABLE
- LEAD CONTACT AND MATERIALS AVAILABILITY
- EXPERIMENTAL MODEL AND SUBJECT DETAILS
  - Animals
  - Human Participants
- METHODS DETAILS
  - Mouse Satellite Cell Isolation
  - FACS Analysis and Cell Sorting
  - Barium Chloride Injury and *In Vivo* Muscle Torque Measurement
  - Cardiotoxin Injury and Transplantation
  - Immunofluorescence Microscopy in Mouse Samples
  - Immunofluorescence Microscopy in Human Samples
  - Image Processing and Analysis
  - RNA-seq Preparation
  - RNA-seq analysis
  - qRT-PCR
  - Statistical Analysis
- DATA AND CODE AVAILABILITY

SUPPLEMENTAL INFORMATION

Supplemental Information can be found online at https://doi.org/10.1016/j.celrep.2019.06.025.

ACKNOWLEDGMENTS

We thank Angus Lindsay, Vineesha Kollipara, Tara Mader, Mayank Verma, Alessandro Magli, Yi Ren, and Olivia Recht for technical assistance and Atsushi Asakura and Ken Korach/Andrea Hevener for the Pax7$^{CreERT2/+}$;R26R^{tdTomato} mice and ERα floxed mice, respectively. Bazedoxifene was a gift from Pfizer. We thank the University of Minnesota Genomics Center for providing sequencing series for this paper. We thank Cynthia S. Faraday for graphic design. Our research has been supported by the NIH grants R01-AG031743 (D.A.L.), R01-AR055685 (M.K.), T32-AR007612 (B.C.C., R.W.A., C.W.B., and C.A.C.), and T32-AG0299796 (A.A.L.); the Muscular Dystrophy Association grant MDA351022 (M.K.); a grant from the American Diabetes Association BS-1-15-170 (E.E.S.); a grant from the Office of the Vice President for Research, University of Minnesota (D.A.L.); and grants from the Academy of Finland 275323 (V.K.) and 309504 (E.K.L.). B.C.C. was also supported by a University of Minnesota Interdisciplinary Doctoral Fellowship.

AUTHOR CONTRIBUTIONS

B.C.C. worked on the study design, data collection, analysis, interpretation, and manuscript writing. R.W.A. worked on the study design, data collection, analysis, and interpretation. A.A.L. and C.W.B. contributed to data collection, analysis, and interpretation. C.A.C., N.L.N, and E.E.S. contributed to data collection and analysis. N.X. worked on data analysis and interpretation. H.-K.J. worked on human experiments and analysis. E.K.L. contributed to the human study design, experiments, analysis, and financial support. S.S. worked on the human study design, experiments, and analysis. V.K. contributed to the human study design, experiments, and financial support. M.K. contributed to the study design, data interpretation, manuscript writing, and financial support. D.A.L. contributed to the conception and design, data interpretation, manuscript writing, and financial support.

DECLARATION OF INTERESTS

The authors declare no competing interests.

Received: May 18, 2018
Revised: April 24, 2019
Accepted: June 5, 2019
Published: July 9, 2019

REFERENCES

Andersson, A., Bernardi, A.I., Nurkkala-Karlsson, M., Stubelius, A., Grahnemo, L., Ohlsson, C., Carlsten, H., and Islander, U. (2016). Suppression of Experimental Arthritis and Associated Bone Loss by a Tissue-Selective Estrogen Complex. Endocrinology *157*, 1013–1020.

Arpke, R.W., and Kyba, M. (2016). Flow Cytometry and Transplantation-Based Quantitative Assays for Satellite Cell Self-Renewal and Differentiation. Methods Mol. Biol. *1460*, 163–179.

Arpke, R.W., Darabi, R., Mader, T.L., Zhang, Y., Toyama, A., Lonetree, C.L., Nash, N., Lowe, D.A., Perlingeiro, R.C., and Kyba, M. (2013). A new immuno-, dystrophin-deficient model, the NSG-mdx(4Cv) mouse, provides evidence for functional improvement following allogeneic satellite cell transplantation. Stem Cells *31*, 1611–1620.

Baber, R.J., Panay, N., and Fenton, A.; IMS Writing Group (2016). 2016 IMS Recommendations on women's midlife health and menopause hormone therapy. Climacteric *19*, 109–150.

Baltgalvis, K.A., Call, J.A., Nikas, J.B., and Lowe, D.A. (2009). Effects of prednisolone on skeletal muscle contractility in mdx mice. Muscle Nerve *40*, 443–454.

Baltgalvis, K.A., Greising, S.M., Warren, G.L., and Lowe, D.A. (2010). Estrogen regulates estrogen receptors and antioxidant gene expression in mouse skeletal muscle. PLoS ONE *5*, e10164.

Baumann, C.W., Rogers, R.G., Gahlot, N., and Ingalls, C.P. (2014). Eccentric contractions disrupt FKBP12 content in mouse skeletal muscle. Physiol. Rep. *2*, e12081.

Beck, T.J., Fuerst, T., Gaither, K.W., Sutradhar, S., Levine, A.B., Hines, T., Yu, C.-R., Williams, R., Mirkin, S., and Chines, A.A. (2015). The effects of bazedoxifene on bone structural strength evaluated by hip structure analysis. Bone *77*, 115–119.

Bernet, J.D., Doles, J.D., Hall, J.K., Kelly Tanaka, K., Carter, T.A., and Olwin, B.B. (2014). p38 MAPK signaling underlies a cell-autonomous loss of stem cell self-renewal in skeletal muscle of aged mice. Nat. Med. *20*, 265–271.

Boland, R., Vasconsuelo, A., Milanesi, L., Ronda, A.C., and de Boland, A.R. (2008). 17beta-estradiol signaling in skeletal muscle cells and its relationship to apoptosis. Steroids *73*, 859–863.

Börjesson, A.E., Farman, H.H., Movérare-Skrtic, S., Engdahl, C., Antal, M.C., Koskela, A., Tuukkanen, J., Carlsten, H., Krust, A., Chambon, P., et al. (2016). SERMs have substance-specific effects on bone, and these effects are mediated via ERαAF-1 in female mice. Am. J. Physiol. Endocrinol. Metab. *310*, E912–E918.

Bosnakovski, D., Xu, Z., Li, W., Thet, S., Cleaver, O., Perlingeiro, R.C., and Kyba, M. (2008). Prospective isolation of skeletal muscle stem cells with a Pax7 reporter. Stem Cells *26*, 3194–3204.

Brack, A.S., Bildsoe, H., and Hughes, S.M. (2005). Evidence that satellite cell decrement contributes to preferential decline in nuclear number from large fibres during murine age-related muscle atrophy. J. Cell Sci. *118*, 4813–4821.

Brack, A.S., Conboy, M.J., Roy, S., Lee, M., Kuo, C.J., Keller, C., and Rando, T.A. (2007). Increased Wnt signaling during aging alters muscle stem cell fate and increases fibrosis. Science *317*, 807–810.

Bray, N.L., Pimentel, H., Melsted, P., and Pachter, L. (2016). Near-optimal probabilistic RNA-seq quantification. Nat. Biotechnol. *34*, 525–527.

Carlson, M.E., and Conboy, I.M. (2007). Loss of stem cell regenerative capacity within aged niches. Aging Cell *6*, 371–382.

Chakkalakal, J.V., Jones, K.M., Basson, M.A., and Brack, A.S. (2012). The aged niche disrupts muscle stem cell quiescence. Nature *490*, 355–360.

Collins, B.C., Mader, T.L., Cabelka, C.A., Iñigo, M.R., Spangenburg, E.E., and Lowe, D.A. (2018). Deletion of estrogen receptor alpha in skeletal muscle results in impaired contractility in female mice. J. Appl. Physiol *124*, 980–992.

Conboy, I.M., and Rando, T.A. (2002). The regulation of Notch signaling controls satellite cell activation and cell fate determination in postnatal myogenesis. Dev. Cell *3*, 397–409.

Conboy, I.M., Conboy, M.J., Wagers, A.J., Girma, E.R., Weissman, I.L., and Rando, T.A. (2005). Rejuvenation of aged progenitor cells by exposure to a young systemic environment. Nature *433*, 760–764.

Cosgrove, B.D., Gilbert, P.M., Porpiglia, E., Mourkioti, F., Lee, S.P., Corbel, S.Y., Llewellyn, M.E., Delp, S.L., and Blau, H.M. (2014). Rejuvenation of the muscle stem cell population restores strength to injured aged muscles. Nat. Med. *20*, 255–264.

Dall, G.V., Hawthorne, S., Seyed-Razavi, Y., Vieusseux, J., Wu, W., Gustafsson, J.A., Byrne, D., Murphy, L., Risbridger, G.P., and Britt, K.L. (2018). Estrogen receptor subtypes dictate the proliferative nature of the mammary gland. J. Endocrinol. *237*, 323–336.

Deschamps, A.M., Murphy, E., and Sun, J. (2010). Estrogen receptor activation and cardioprotection in ischemia reperfusion injury. Trends Cardiovasc. Med. *20*, 73–78.

Dumont, N.A., Wang, Y.X., and Rudnicki, M.A. (2015). Intrinsic and extrinsic mechanisms regulating satellite cell function. Development *142*, 1572–1581.

Enns, D.L., and Tiidus, P.M. (2008). Estrogen influences satellite cell activation and proliferation following downhill running in rats. J. Appl. Physiol. *104*, 347–353.

Enns, D.L., Iqbal, S., and Tiidus, P.M. (2008). Oestrogen receptors mediate oestrogen-induced increases in post-exercise rat skeletal muscle satellite cells. Acta Physiol. (Oxf.) *194*, 81–93.

Fry, C.S., Lee, J.D., Mula, J., Kirby, T.J., Jackson, J.R., Liu, F., Yang, L., Mendias, C.L., Dupont-Versteegden, E.E., McCarthy, J.J., and Peterson, C.A. (2015). Inducible depletion of satellite cells in adult, sedentary mice impairs muscle regenerative capacity without affecting sarcopenia. Nat. Med. *21*, 76–80.

Fry, C.S., Porter, C., Sidossis, L.S., Nieten, C., Reidy, P.T., Hundeshagen, G., Mlcak, R., Rasmussen, B.B., Lee, J.O., Suman, O.E., et al. (2016). Satellite cell activation and apoptosis in skeletal muscle from severely burned children. J. Physiol. *594*, 5223–5236.

Fukada, S., Uezumi, A., Ikemoto, M., Masuda, S., Segawa, M., Tanimura, N., Yamamoto, H., Miyagoe-Suzuki, Y., and Takeda, S. (2007). Molecular signature of quiescent satellite cells in adult skeletal muscle. Stem Cells *25*, 2448–2459.

Gelsomino, L., Panza, S., Giordano, C., Barone, I., Gu, G., Spina, E., Catalano, S., Fuqua, S., and Andò, S. (2018). Mutations in the estrogen receptor alpha hormone binding domain promote stem cell phenotype through notch activation in breast cancer cell lines. Cancer Lett. *428*, 12–20.

Greising, S.M., Baltgalvis, K.A., Lowe, D.A., and Warren, G.L. (2009). Hormone therapy and skeletal muscle strength: a meta-analysis. J. Gerontol. A Biol. Sci. Med. Sci. *64*, 1071–1081.

Greising, S.M., Baltgalvis, K.A., Kosir, A.M., Moran, A.L., Warren, G.L., and Lowe, D.A. (2011). Estradiol's beneficial effect on murine muscle function is independent of muscle activity. J. Appl. Physiol. *110*, 109–115.

Guo, L., Xu, J., Qi, J., Zhang, L., Wang, J., Liang, J., Qian, N., Zhou, H., Wei, L., and Deng, L. (2013). MicroRNA-17-92a upregulation by estrogen leads to Bim targeting and inhibition of osteoblast apoptosis. J. Cell Sci. *126*, 978–988.

Hamilton, D.J., Minze, L.J., Kumar, T., Cao, T.N., Lyon, C.J., Geiger, P.C., Hsueh, W.A., and Gupte, A.A. (2016). Estrogen receptor alpha activation enhances mitochondrial function and systemic metabolism in high-fat-fed ovariectomized mice. Physiol. Rep. *4*, e12913.

Harlow, S.D., Gass, M., Hall, J.E., Lobo, R., Maki, P., Rebar, R.W., Sherman, S., Sluss, P.M., and de Villiers, T.J.; STRAW 10 Collaborative Group (2012). Executive summary of the Stages of Reproductive Aging Workshop + 10: addressing the unfinished agenda of staging reproductive aging. Menopause *19*, 387–395.

Hewitt, S.C., Kissling, G.E., Fieselman, K.E., Jayes, F.L., Gerrish, K.E., and Korach, K.S. (2010). Biological and biochemical consequences of global deletion of exon 3 from the ER alpha gene. FASEB J *24*, 4660–4667.

Hindi, S.M., and Kumar, A. (2016). TRAF6 regulates satellite stem cell self-renewal and function during regenerative myogenesis. J. Clin. Invest. *126*, 151–168.

Hirai, H., Verma, M., Watanabe, S., Tastad, C., Asakura, Y., and Asakura, A. (2010). MyoD regulates apoptosis of myoblasts through microRNA-mediated down-regulation of Pax3. J. Cell Biol. *191*, 347–365.

Kamanga-Sollo, E., White, M.E., Hathaway, M.R., Weber, W.J., and Dayton, W.R. (2010). Effect of Estradiol-17beta on protein synthesis and degradation rates in fused bovine satellite cell cultures. Domest. Anim. Endocrinol. *39*, 54–62.

Keefe, A.C., Lawson, J.A., Flygare, S.D., Fox, Z.D., Colasanto, M.P., Mathew, S.J., Yandell, M., and Kardon, G. (2015). Muscle stem cells contribute to myofibres in sedentary adult mice. Nat. Commun. *6*, 7087.

Kim, J.H., Han, G.C., Seo, J.Y., Park, I., Park, W., Jeong, H.W., Lee, S.H., Bae, S.H., Seong, J., Yum, M.K., et al. (2016). Sex hormones establish a reserve pool of adult muscle stem cells. Nat. Cell Biol. *18*, 930–940.

Kim, S., Ko, Y., Lee, H.J., and Lim, J.E. (2018). Menopausal hormone therapy and the risk of breast cancer by histological type and race: a meta-analysis of randomized controlled trials and cohort studies. Breast Cancer Res. Treat. *170*, 667–675.

Kitajima, Y., and Ono, Y. (2016). Estrogens maintain skeletal muscle and satellite cell functions. J. Endocrinol. *229*, 267–275.

Kitajima, Y., Doi, H., Ono, Y., Urata, Y., Goto, S., Kitajima, M., Miura, K., Li, T.-S., and Masuzaki, H. (2015). Estrogen deficiency heterogeneously affects tissue specific stem cells in mice. Sci. Rep. *5*, 12861.

Kosir, A.M., Mader, T.L., Greising, A.G., Novotny, S.A., Baltgalvis, K.A., and Lowe, D.A. (2015). Influence of ovarian hormones on strength loss in healthy and dystrophic female mice. Med. Sci. Sports Exerc. *47*, 1177–1187.

Kovanen, A., Aukee, P., Kokko, K., Finni, T., Tarkka, I.M., Tammelin, T., Kujala, U.M., Sipilä, S., and Laakkonen, E.K. (2018). Design and protocol of Estrogenic Regulation of Muscle Apoptosis (ERMA) study with 47 to 55-year-old women's cohort: novel results show menopause-related differences in blood count. Menopause *25*, 1020–1032.

Kuang, S., Kuroda, K., Le Grand, F., and Rudnicki, M.A. (2007). Asymmetric self-renewal and commitment of satellite stem cells in muscle. Cell *129*, 999–1010.

La Colla, A., Pronsato, L., Milanesi, L., and Vasconsuelo, A. (2015). 17β-Estradiol and testosterone in sarcopenia: Role of satellite cells. Ageing Res. Rev. *24* (*Pt B*), 166–177.

La Colla, A., Vasconsuelo, A., Milanesi, L., and Pronsato, L. (2017). 17beta-Estradiol Protects Skeletal Myoblasts from Apoptosis through P53, BCL-2 and FoxO Families. J. Cell. Biochem. *118*, 104–115.

Laakkonen, E.K., Kulmala, J., Aukee, P., Hakonen, H., Kujala, U.M., Lowe, D.A., Kovanen, V., Tammelin, T., and Sipilä, S. (2017). Female reproductive factors are associated with objectively measured physical activity in middle-aged women. PLoS ONE *12*, e0172054.

Lai, S., Collins, B.C., Colson, B.A., Kararigas, G., and Lowe, D.A. (2016). Estradiol modulates myosin regulatory light chain phosphorylation and contractility in skeletal muscle of female mice. Am. J. Physiol. Endocrinol. Metab. *310*, E724–E733.

Le, G., Novotny, S.A., Mader, T.L., Greising, S.M., Chan, S.S.K., Kyba, M., Lowe, D.A., and Warren, G.L. (2018). A moderate oestradiol level enhances neutrophil number and activity in muscle after traumatic injury but strength recovery is accelerated. J. Physiol. *596*, 4665–4680.

Lowe, D.A., Warren, G.L., Ingalls, C.P., Boorstein, D.B., and Armstrong, R.B. (1995). Muscle function and protein metabolism after initiation of eccentric contraction-induced injury. J. Appl. Physiol. *79*, 1260–1270.

McClung, J.M., Davis, J.M., and Carson, J.A. (2007). Ovarian hormone status and skeletal muscle inflammation during recovery from disuse in rats. Exp. Physiol. *92*, 219–232.

Metsalu, T., and Vilo, J. (2015). ClustVis: a web tool for visualizing clustering of multivariate data using Principal Component Analysis and heatmap. Nucleic Acids Res. *43* (*W1*), W566–W570.

Moran, A.L., Nelson, S.A., Landisch, R.M., Warren, G.L., and Lowe, D.A. (2007). Estradiol replacement reverses ovariectomy-induced muscle contractile and myosin dysfunction in mature female mice. J. Appl. Physiol. *102*, 1387–1393.

Murphy, M.M., Lawson, J.A., Mathew, S.J., Hutcheson, D.A., and Kardon, G. (2011). Satellite cells, connective tissue fibroblasts and their interactions are crucial for muscle regeneration. Development *138*, 3625–3637.

Murphy, M.M., Keefe, A.C., Lawson, J.A., Flygare, S.D., Yandell, M., and Kardon, G. (2014). Transiently active Wnt/β-catenin signaling is not required but must be silenced for stem cell function during muscle regeneration. Stem Cell Rep. *3*, 475–488.

Nelson, L.R., and Bulun, S.E. (2001). Estrogen production and action. J. Am. Acad. Dermatol. *45*, S116–S124.

Nelson, J.F., Felicio, L.S., Randall, P.K., Sims, C., and Finch, C.E. (1982). A longitudinal study of estrous cyclicity in aging C57BL/6J mice: I. Cycle frequency, length and vaginal cytology. Biol. Reprod. *27*, 327–339.

Pallafacchina, G., Blaauw, B., and Schiaffino, S. (2013). Role of satellite cells in muscle growth and maintenance of muscle mass. Nutr. Metab. Cardiovasc. Dis. *23* (*Suppl 1*), S12–S18.

Phillips, S.K., Rook, K.M., Siddle, N.C., Bruce, S.A., and Woledge, R.C. (1993). Muscle weakness in women occurs at an earlier age than in men, but strength is preserved by hormone replacement therapy. Clin. Sci. (Lond.) *84*, 95–98.

Phillips, S.K., Sanderson, A.G., Birch, K., Bruce, S.A., and Woledge, R.C. (1996). Changes in maximal voluntary force of human adductor pollicis muscle during the menstrual cycle. J. Physiol. *496*, 551–557.

Qaisar, R., Renaud, G., Hedstrom, Y., Pöllänen, E., Ronkainen, P., Kaprio, J., Alen, M., Sipilä, S., Artemenko, K., Bergquist, J., et al. (2013). Hormone replacement therapy improves contractile function and myonuclear organization of single muscle fibres from postmenopausal monozygotic female twin pairs. J. Physiol. *591*, 2333–2344.

Rader, E.P., and Faulkner, J.A. (2006). Effect of aging on the recovery following contraction-induced injury in muscles of female mice. J. Appl. Physiol. *101*, 887–892.

Ribas, V., Nguyen, M.T., Henstridge, D.C., Nguyen, A.K., Beaven, S.W., Watt, M.J., and Hevener, A.L. (2010). Impaired oxidative metabolism and inflammation are associated with insulin resistance in ERalpha-deficient mice. Am. J. Physiol. Endocrinol. Metab. *298*, E304–E319.

Ribas, V., Drew, B.G., Zhou, Z., Phun, J., Kalajian, N.Y., Soleymani, T., Daraei, P., Widjaja, K., Wanagat, J., de Aguiar Vallim, T.Q., et al. (2016). Skeletal muscle action of estrogen receptor α is critical for the maintenance of mitochondrial function and metabolic homeostasis in females. Sci. Transl. Med. *8*, 334ra54.

Ronda, A.C., Vasconsuelo, A., and Boland, R. (2013). 17β-estradiol protects mitochondrial functions through extracellular-signal-regulated kinase in C2C12 muscle cells. Cell. Physiol. Biochem. *32*, 1011–1023.

Sajko, S., Kubínová, L., Cvetko, E., Kreft, M., Wernig, A., and Eržen, I. (2004). Frequency of M-cadherin-stained satellite cells declines in human muscles during aging. J. Histochem. Cytochem. *52*, 179–185.

Sambasivan, R., Yao, R., Kissenpfennig, A., Van Wittenberghe, L., Paldi, A., Gayraud-Morel, B., Guenou, H., Malissen, B., Tajbakhsh, S., and Galy, A. (2011). Pax7-expressing satellite cells are indispensable for adult skeletal muscle regeneration. Development *138*, 3647–3656.

Sanchez, A.M., Candau, R.B., and Bernardi, H. (2014). FoxO transcription factors: their roles in the maintenance of skeletal muscle homeostasis. Cell. Mol. Life Sci. *71*, 1657–1671.

Schultz, E., Jaryszak, D.L., Gibson, M.C., and Albright, D.J. (1986). Absence of exogenous satellite cell contribution to regeneration of frozen skeletal muscle. J. Muscle Res. Cell Motil. *7*, 361–367.

Severson, T.M., Kim, Y., Joosten, S.E.P., Schuurman, K., van der Groep, P., Moelans, C.B., Ter Hoeve, N.D., Manson, Q.F., Martens, J.W., van Deurzen, C.H.M., et al. (2018). Characterizing steroid hormone receptor chromatin binding landscapes in male and female breast cancer. Nat. Commun. *9*, 482.

Shea, K.L., Xiang, W., LaPorta, V.S., Licht, J.D., Keller, C., Basson, M.A., and Brack, A.S. (2010). Sprouty1 regulates reversible quiescence of a self-renewing adult muscle stem cell pool during regeneration. Cell Stem Cell *6*, 117–129.

Shefer, G., Van de Mark, D.P., Richardson, J.B., and Yablonka-Reuveni, Z. (2006). Satellite-cell pool size does matter: defining the myogenic potency of aging skeletal muscle. Dev. Biol. *294*, 50–66.

Soneson, C., Love, M., and Robinson, M. (2015). Differential analyses for RNA-seq: transcript-level estimates improve gene-level inferences. F1000Res *4*, 1521.

Sousa-Victor, P., Gutarra, S., García-Prat, L., Rodriguez-Ubreva, J., Ortet, L., Ruiz-Bonilla, V., Jardí, M., Ballestar, E., González, S., Serrano, A.L., et al. (2014). Geriatric muscle stem cells switch reversible quiescence into senescence. Nature *506*, 316–321.

Taaffe, D.R., Sipilä, S., Cheng, S., Puolakka, J., Toivanen, J., and Suominen, H. (2005). The effect of hormone replacement therapy and/or exercise on skeletal muscle attenuation in postmenopausal women: a yearlong intervention. Clin. Physiol. Funct. Imaging *25*, 297–304.

Thomas, A., Bunyan, K., and Tiidus, P.M. (2010). Oestrogen receptor-alpha activation augments post-exercise myoblast proliferation. Acta Physiol. (Oxf.) *198*, 81–89.

Toth, M.J., Poehlman, E.T., Matthews, D.E., Tchernof, A., and MacCoss, M.J. (2001). Effects of estradiol and progesterone on body composition, protein synthesis, and lipoprotein lipase in rats. Am. J. Physiol. Endocrinol. Metab *280*, E496–E501.

Troy, A., Cadwallader, A.B., Fedorov, Y., Tyner, K., Tanaka, K.K., and Olwin, B.B. (2012). Coordination of satellite cell activation and self-renewal by Par-complex-dependent asymmetric activation of p38α/β MAPK. Cell Stem Cell *11*, 541–553.

Vasconsuelo, A., Milanesi, L., and Boland, R. (2008). 17Beta-estradiol abrogates apoptosis in murine skeletal muscle cells through estrogen receptors: role of the phosphatidylinositol 3-kinase/Akt pathway. J. Endocrinol. *196*, 385–397.

Vasconsuelo, A., Milanesi, L., and Boland, R. (2010). Participation of HSP27 in the antiapoptotic action of 17beta-estradiol in skeletal muscle cells. Cell Stress Chaperones *15*, 183–192.

Verdijk, L.B., Dirks, M.L., Snijders, T., Prompers, J.J., Beelen, M., Jonkers, R.A., Thijssen, D.H., Hopman, M.T., and Van Loon, L.J. (2012). Reduced satellite cell numbers with spinal cord injury and aging in humans. Med. Sci. Sports Exerc. *44*, 2322–2330.

Verdijk, L.B., Snijders, T., Drost, M., Delhaas, T., Kadi, F., and van Loon, L.J. (2014). Satellite cells in human skeletal muscle; from birth to old age. Age (Dordr.) *36*, 545–547.

Wood, G.A., Fata, J.E., Watson, K.L.M., and Khokha, R. (2007). Circulating hormones and estrous stage predict cellular and stromal remodeling in murine uterus. Reproduction *133*, 1035–1044.

Zhou, Z., Ribas, V., Rajbhandari, P., Drew, B.G., Moore, T.M., Fluitt, A.H., Reddish, B.R., Whitney, K.A., Georgia, S., Vergnes, L., et al. (2018). Estrogen receptor α protects pancreatic β-cells from apoptosis by preserving mitochondrial function and suppressing endoplasmic reticulum stress. J. Biol. Chem. *293*, 4735–4751.

STAR★METHODS

KEY RESOURCES TABLE

REAGENT or RESOURCE	SOURCE	IDENTIFIER
Antibodies		
PE-Cy7 rat anti-mouse CD31 (clone 390)	BD Biosciences	Cat# 561410 ; RRID:AB_10612003
PE-Cy7 rat anti-mouse CD45 (clone 30-F11)	BD Biosciences	Cat# 552848 ; RRID:AB_394489
Biotin rat anti-mouse CD106 (clone 429(MVCAM.A)	BD Biosciences	Cat# 553331; RRID:AB_394787
PE Streptavidin	BD Biosciences	Cat# 554061; RRID:AB_10053328
Itga7 647 (clone R2F2)	AbLab	Cat# AB000000274
Anti-Pax7 mouse IgG1	DSHB	Cat# PAX7
Gt anti-mouse biotin-conjugated secondary	Jackson Immuno Research Laboratories	Cat# 115-065-205 ; RRID:AB_2338571
Anti-laminin rabbit	Sigma-Aldrich	Cat# L9393 ; RRID:AB_477163
Gt anti-rabbit Alexa 488 secondary	Life Technologies	Cat# A11034 ; RRID:AB_2576217
Anti-RFP rabbit polyclonal	Rockland Immunochemicals Inc	Cat# 600-401-379 ; RRID:AB_2209751
Anti-laminin mouse	Sigma-Aldrich	Cat# Clone LAM-89 ; RRID:AB_477162
Gt anti-mouse Alexa 555	Life Technologies	Cat# A-21422 ; RRID:AB_2535844
Chemicals, Peptides, and Recombinant Proteins		
Collagenase Type II	GIBCO	Cat# 17101-015
Dulbecco's modified Eagle's medium (DMEM) without phenol red containing 4.00 mM L-glutamine, 4,500 mg/L glucose, and sodium pyruvate	Hyclone	Cat# SH30284.01
Ham's/F-10 Media	Hyclone	Cat# SH30025.01
Horse Serum	GIBCO	Cat# 26050088
HEPES Buffer	GIBCO	Cat# 15630080
Pen/Strep	GIBCO	Cat# 15140122
Dispase	GIBCO	Cat# 17105-041
Fetal Bovine Serum	GIBCO	Cat# 16000044
Tamoxifen (TMX)	Sigma-Aldrich	Cat# T5648
Cardiotoxin (CTX)	Sigma-Aldrich	Cat# 217503
$BaCl_2$	Sigma-Aldrich	Cat#B-0750
2-methylbutane	Sigma-Aldrich	Cat# M32631
Bovine Serum Albumin (BSA)	Sigma-Aldrich	Cat# A2153
Prolong gold antifade mountant with DAPI	Life Technologies	Cat# P36931
Paraformaldehyde (PFA)	Sigma-Aldrich	Cat# 158127
Triton X-100	Sigma-Aldrich	Cat# X-100
Prolong gold antifade mountant media no DAPI	Life Technologies	Cat# P10144
TNB-buffer	PerkinElmer	Cat# FP1020
Bazedoxifine	Pfizer	Cas# 198481-33-3
Critical Commercial Assays		
In Situ Cell Death, Fluorescein Detection Kit	Roche Diagnostics	Cat# 11684795910
Vectastain ABC kit	Vector Laboratories	Cat# PK-6100
Tyramide Signal Amplification (TSA) Plus Cyanine 3 kit	PerkinElmer	Cat# NEL744
SUPERVILO cDNA Synthesis kit	ThermoFisher	Cat# 11756050
Direct-Zol MicroPrep Kit	Zymo Research Labs	Cat# R2061
Red-taq Ready Mix	Sigma-Adlrich	R2523

(*Continued on next page*)

Continued

REAGENT or RESOURCE	SOURCE	IDENTIFIER
GoTaq_ qPCR Master Mix	Promega	A6001
Quant-iT RiboGreen_ RNA Assay Kit Scientific	ThermoFisher	R11490
SMARTer Stranded Total RNA-Seq-Pico Mammalian Kit	Clontech	635007
Experimental Models: Organisms/Strains		
Mouse: *C57/BL6*	Jackson Laboratories	JAX: 000664
Mouse: *Pax7-ZsGreen*	Bosnakovski et al., 2008	N/A
Mouse: *B6.Cg-*$^{Pax7tm1(cre/ERT2)Gaka}$*/J*	Jackson Laboratories	JAX: 017763
Mouse: *B6.Cg-Gt(ROSA)*$^{26Sortm9(CAG-tdTomato)Hze}$*/J*	Jackson Laboratories	JAX: 007909
Mouse: *ER*α*Exon3*$^{fl/fl}$	Hewitt et al., 2010	N/A
Oligonucleotides		
Primer Sequences	See Table S1	N/A
Software and Algorithms		
Prism 7	GraphPad	RRID:SCR_002798
FlowJo 10	FLOWJO, LLC	RRID: SCR_008520
SigmaPlot 12.5	Systat Software Inc	RRID:SCR_010455
SPSS 24	IBM Corporation	RRID:SCR_002865
ImageJ	NIH	RRID:SCR_003070
ClustVis	Metsalu and Vilo, 2015	N/A
Ingenuity Pathway Analysis	QIAGEN	N/A
Deposited Data		
RNA-seq for transcriptome analysis of ZsGreen+ cells from *Pax7*$^{+/+}$*Esr1*$^{fl/fl}$*;Pax7-ZsGreen* and *Pax7*$^{CreERT2/+}$*; Esr1*$^{fl/fl}$*; Pax7-ZsGreen*	In this study	GEO: GSE126872

LEAD CONTACT AND MATERIALS AVAILABILITY

Further information and requests for resources and reagents should be directed to and will be fulfilled by the Lead Contact, Dawn Lowe (lowex017@umn.edu).

EXPERIMENTAL MODEL AND SUBJECT DETAILS

Animals

Animal experiments in this study were performed in accordance with protocols approved by the Institutional Animal Care and Use Committee at the University of Minnesota. All experiments were conducted on female mice when they were young adults (3-4 mo of age). Satellite cells were harvested from C57/BL6 (Purchased from Jackson Laboratories, 000664) and Pax7-ZsGreen mice that were either control or ovariectomized (bilateral removal of the ovaries) and sacrificed 2, 3.5, or 7 mo post-surgery (n = 5 mice for each group). ER$\alpha^{fl/fl}$ mice were ovariectomized (Ovx) and half received a 0.18 mg 60-day slow-release 17β-estradiol (Ovx+E_2) pellet via trochar implantation (n = 3-4 mice) (Moran et al., 2007). For strength experiments, C57/BL6 mice were ovariectomized and half received placebo pellets (Ovx+placebo) and half received 0.18 mg 60-day slow-release 17β-estradiol pellets (Ovx+E_2) (n = 6-8 mice). For Bazedoxifine experiments, C57/BL6 mice were ovariectomized and half received placebo pellets (Ovx+placebo) and half received 1.44 mg Bazedoxifine (Ovx+BZA) pellets (n = 5-6 mice) (Andersson et al. 2016). For transplant experiments, female *Pax7-ZsGreen* and *Pax7*$^{CreERT2/+}$*;R26R*^{tdTomato} mice were donors and were age-matched to female C57/BL6 recipient mice (n = 6-15 mice for each experiment); a subset of recipients was ovariectomized. *Pax7*$^{CreERT2/+}$*; Esr1*$^{fl/fl}$*;Pax7-ZsGreen* (scERαKO) and *Pax7*$^{+/+}$*Esr1*$^{fl/fl}$*;Pax7-ZsGreen* (scERαWT) were generated in-house. Female scERαWT and scERαKO mice were treated with 2mg tamoxifen for 5 d consecutively (Keefe et al., 2015; Murphy et al., 2011). Two mo after tamoxifen treatment, mice were used for satellite cell harvests (n = 6 mice) and transplantation (n = 6 mice). For all experiments, the estrous cycle was tracked for 3-5 d consecutively via vaginal cytology to confirm mice had normal estrous cycles or had ceased cycling for those that were Ovx (Nelson et al., 1982). Uterine mass was measured at the time of sacrifice as a second verification of successful ovariectomy surgery or estradiol treatment (Wood et al., 2007). Uterine mass across all experiments for control, Ovx, and Ovx+E_2 mice averaged (SEM): 101.7 (5.1), 13.5 (0.7), and 207.9 (27.0) mg, respectively.

Human Participants

Brieflyparticipants were instructed to wear monitors on the right hip during waking hours for seven consecutive days. Moderate to vigorous intensity physical activity (MVPA) was defined by using tri-axial vector magnitude cut-point over 2690 counts per minute (cpm) to define the cut-point for at least moderate intensity level. There were small intra-individual differences in wearing times of the accelerometer (mean wearing time 15.2 ± 0.3 hours/day across 6.8 ± 0.2 days). Thereforethe MVPA time (min/day) was normalized by wearing time to correspond daily 16 hour waking time. The Ethics Committee of the Central Finland Health Care District approved the ERMA Study in 2014 (K-S shp Dnro U/2014). An informed consent was given by each participant at the laboratory before any sampling or measurement was done. Altogetherthe study protocol followed good clinical and scientific practice and the Declaration of Helsinki, 2018Muscle samples from the Estrogenic Regulation of Muscle Apoptosis (ERMA) Study were analyzed for satellite cells (n = 5 women). The ERMA study is a population-based longitudinal cohort study comprised of women 47 to 55 years of age living in the city of Jyväskylä and the neighboring municipalities in Finland (Kovanen et al., 2018). Systemic follicle stimulating hormone (FSH) and 17β-estradiol levels were immunoassayed by IMMULITE® 2000 XPi System (Siemens Healthcare Diagnostics, UK) from the fasting blood samples taken from the antecubital vein in a supine position between 7:00 and 10:00 AM. Participants were assigned to menopausal groups using these hormone results, along with information from menstrual cycle diaries, following guidelines established by Stages of Reproductive Aging Workshop (STRAW+10; Harlow et al., 2012). Percentage of body fat and lean body mass was assessed by a multifrequency bioelectrical impedance analyzer (InBody™ 720; Biospace, Seoul, Korea) after overnight fasting with the participant wearing only undergarments. Physical activity was assessed with ActiGraph accelerometers (Pensacola, Florida, USA) as in Laakkonen et al. (2017). Briefly, participants were instructed to wear monitors on the right hip during waking hours for seven consecutive days. Moderate to vigorous intensity physical activity (MVPA) was defined by using tri-axial vector magnitude cut-point over 2690 counts per minute (cpm) to define the cut-point for at least moderate intensity level. There were small intra-individual differences in wearing times of the accelerometer (mean wearing time 15.2 ± 0.3 hours/day across 6.8 ± 0.2 days). Therefore, the MVPA time (min/day) was normalized by wearing time to correspond daily 16 hour waking time. The Ethics Committee of the Central Finland Health Care District approved the ERMA Study in 2014 (K-S shp Dnro U/2014). An informed consent was given by each participant at the laboratory before any sampling or measurement was done. Altogether, the study protocol followed good clinical and scientific practice and the Declaration of Helsinki.

METHODS DETAILS

Mouse Satellite Cell Isolation

Isolation of satellite cells from single skeletal muscles (e.g., gastrocnemius) was performed as described previously (Arpke and Kyba, 2016). Muscles were carefully dissected and chopped in parallel with muscle fibers using razor blade and forceps to separate the fibers. Muscles were incubated shaking for 75 min in 0.2% collagenase type II (17101-015, GIBCO, Grand Island, NY) in high glucose Dulbecco's modified Eagle's medium (DMEM) without phenol red containing 4.00 mM L-glutamine, 4,500 mg/L glucose, and sodium pyruvate (SH30284.01, Hyclone, Logan, UT) supplemented with 1% Pen/Strep (15140122, GIBCO) at 37°C. Samples were washed with Rinsing Solution (F-10+), Ham's/F-10 medium (SH30025.01, HyClone) supplemented with 10% Horse serum, 1% HEPES buffer solution (15630080, GIBCO) and 1% Pen/Strep (GIBCO) and centrifuged at 1500 rpm x 5min at 4°C. Samples were washed and centrifuged a second time. Samples were pulled into a sheared Pasteur pipette, centrifuged and washed again. Following aspiration, samples were resuspended in F-10+ with collagenase collagenase type II and dispase (17105-041, GIBCO), vortexed and incubated shaking at 37°C for 30 min. Samples were vortexed again, drawn and released into a 3 mL syringe with 16-gauge needle four times then with an 18-gauge needle four times and passed through a 40-μm cell strainer (Falcon, Hanover Park, IL). 3 mL of F-10+ was added to each sample and centrifuged at 1500 rpm x 5min 4°C. Following aspiration, samples were resuspended in FACS staining medium (2% FBS in PBS). Bulk isolation (hindlimb muscles excluding soleus, triceps muscles, and psoas muscles) of satellite cells was performed similarly and as described previously (Arpke et al., 2013).

FACS Analysis and Cell Sorting

Muscle samples were stained using an antibody mixture of PE-Cy7 rat anti-mouse CD31 (clone 390), PE-Cy7 rat anti-mouse CD45 (clone 30-F11), Biotin rat anti-mouse CD106 (clone 429(MVCAM.A)) and PE Streptavidin from BD Biosciences (San Diego, CA); and Itga7 647 (clone R2F2) from AbLab (Vancouver, B.C., Canada). Antibody cocktail was added to samples and incubated on ice for 30 min. Samples were washed and resuspended with FACS staining media containing propidium iodide for FACS analysis on the FACSAriaII SORP (BD Biosciences, San Diego, CA). Total satellite cells (lineage negative; VCAM,alpha7 double positive cells or ZsGreen+) (Figures S1A and S1B) were analyzed while draining the entire sample from each skeletal muscle sample. For transplanted tibialis anterior (TA) muscles, the number of donor (ZsGreen + or tdTOM+) satellite cells were examined as previously described (Arpke et al., 2013).

Barium Chloride Injury and *In Vivo* Muscle Torque Measurement

As previously described (Baltgalvis et al., 2009; Baumann et al., 2014; Lowe et al., 1995), contractile function of the left anterior crural muscles was measured *in vivo* immediately before the injuries, as well as 7, 14, and 21 days after each injury. Briefly, anesthetized mice (1.25% isoflurane and 125 mL O_2 per minute) were placed on a temperature-controlled platform to maintain core body

temperature between 35 and 37°C. The left knee was clamped and the left foot was secured to an aluminum "shoe" that is attached to the shaft of an Aurora Scientific 300B servomotor (Aurora Scientific, ON, Canada). Sterilized platinum needle electrodes were inserted through the skin for stimulation of the left common peroneal nerve. Stimulation voltage and needle electrode placement were optimized with 5–15 isometric contractions (200 ms train of 0.1 ms pulses at 200 Hz). Two minutes following optimization, contractile function of the anterior crural muscles was assessed by measuring isometric torque as a function of stimulation frequency (20–300 Hz), with the highest recorded torque defined as maximal isometric torque. Following pre-injury and 21 day torque measurements, barium chloride (1.2% in sterile demineralized water) (Ricca Chemical Company, Arlington, TX) was injected into the tibialis anterior muscle of each mouse with a Hamilton syringe similar to Murphy et al. (2014). Functional torque measurements were performed on the same groups of mice at each time-point post-injury, and expressed relative to pre-injury maximal isometric torque.

Cardiotoxin Injury and Transplantation

Transplant recipient mice were anesthetized with 150 mg/kg ketamine plus 10 mg/kg xylazine and both hind limbs were subjected to a 900 cGy dose of irradiation using an RS 2000 Biological Research Irradiator (Rad Source Technologies, Inc., Suwanee, GA). Lead shields limited exposure to the hind limbs only. 24 h following irradiation, 15 μL of cardiotoxin (10 μM in PBS, Sigma-Aldrich, Saint Louis, MO) was injected into both TA muscles of each mouse with a Hamilton syringe. 24 h following cardiotoxin injection, 600 ZsGreen+ cells were resuspended into 10 μL of sterile saline and injected into both TA's. Both TA's were harvested 1 mo post-transplantation and prepared for FACS analysis as described above. When tdTom+ cells were transplanted, one TA was harvested and prepared for FACS analysis and the contralateral TA was harvested and prepared for sectioning and staining.

Immunofluorescence Microscopy in Mouse Samples

TA muscles were removed and placed in OCT compound, frozen in 2-methylbutane (Sigma-Aldrich) cooled by liquid nitrogen and stored at −80°C until use. For visualization of satellite cells and apoptotic cells in skeletal muscle, Pax7 and terminal deoxynucleotidyl transferase dUTP nick end labeling (TUNEL) staining was performed on 7 μM cryosections (CM 1850, Leica Microsystems, Buffalo Grove, IL). TUNEL was detected using *In Situ* Cell Death, Fluorescein Detection Kit according to manufacturer's instructions (11684795910, Roche Diagnostics, Mannheim, Germany). Following TUNEL, Pax7 staining was completed as previously reported (Keefe et al., 2015; Murphy et al., 2011). In brief, slides were incubated in citrate buffer for 10 min and then antigen retrieval was performed by microwaving at 20 s intervals for a total of 3 min in citrate buffer. Slides were washed two times in 1x PBS for 2 min each and blocked in 3% bovine serum albumin (BSA) for 1 h at room temperature. Slides were incubated with anti-pax7 mouse IgG1 primary antibody (PAX7, Developmental Hybridoma Bank at Iowa University, 1:20 in 3% BSA) overnight at 4°C. Slides were incubated with goat anti-mouse biotin-conjugated secondary antibody (115-065-205, Jackson Immuno Research Laboratories Inc, West Grove, PA, 1:1000 in 3% BSA) for 1 h at room temperature. Visualization of the primary antibody was performed using the Vectastain ABC kit (PK-6100, Vector Laboratories, Burlingame, CA) and Tyramide Signal Amplification (TSA) Plus Cyanine 3 kit (NEL744, PerkinElmer, Waltham, MA, 1:50 in diluent buffer). Slides were washed again and then prolong gold antifade mountant with DAPI (P36931, Life technologies, Grand Island, NY) was applied and coverslip added.

For determination of the cross-sectional area of the TA muscle and to determine the myofiber border, adjacent 7 μm sections of each mouse sample were cryo-sectioned. Samples were fixed in 4% PFA for 10 min, washed with 1x PBS and blocked with 3% BSA in 1x PBS for 60 min at room temperature. Sections were incubated overnight at 4°C with primary antibody anti-laminin (L9393; Sigma-Aldrich, 1:250) diluted in 1% BSA in 1x PBS. Slides were washed with 1x PBS and secondary antibody Alexa 488 goat anti-rabbit (A11034; Life Technologies, 1:500) was applied for 1 h at room temperature. Slides were washed and then mounted with Prolong Gold Anti-fade mountant media (Life Technologies).

For visualization of fiber engraftment following transplantation, 10 μM sections of TA muscles were cryosectioned. Samples were fixed in 2% paraformaldehyde (PFA) for 5 min, washed with 0.01% triton in 1x PBS, permeabilized with 0.2% triton for 5 min, and then blocked with 1% BSA in wash buffer for 30 min at room temperature. Sections were incubated overnight at 4°C with primary antibodies diluted in 1% BSA in wash buffer simultaneously; rabbit polyclonal anti-RFP (600-401-379, Rockland Immunochemicals Inc, Pottstown, PA, 1:200) and mouse monoclonal anti-laminin (Clone LAM-89; Sigma-Aldrich, 1:250). Slides were washed with wash buffer and secondary antibodies were applied for 1 h at room temperature simultaneously, Alexa 555 goat anti-mouse and Alexa 480 goat anti-rabbit IgG (A-21422 and A-11034, 1:500; Life Technologies). Slides were washed and then mounted with prolong gold anti-fade mountant media (P10144, Life Technologies).

Immunofluorescence Microscopy in Human Samples

Needle muscle biopsies were obtained under local anesthesia from vastus lateralis of five women when they were perimenopausal and then again after being classified as postmenopausal. Visible connective, adipose tissue and blood was removed before the biopsy sample was embedded in Tissue Tek compound and frozen in 2-methylbutane (Sigma-Aldrich) cooled in liquid nitrogen and stored at −150°C until use. Pax7 positive cells were identified on 10 μm cryosections (CM 3000, Leica Instruments). In brief, slides were incubated in citrate buffer for 10 min and then antigen retrieval was performed by microwaving for 4 min in citrate buffer. Slides cooled for 5 min and were washed with 1x PBS. Blocking was done in 2% TNB-buffer (Blocking reagent, FP1020, PerkinElmer) for 1 h at room temperature. Slides were incubated with anti-pax7 mouse IgG1 primary antibody (PAX7, Developmental Hybridoma Bank at Iowa University, 1:25 in 2% TNB) overnight at 4°C. Slides were incubated with goat anti-mouse biotin-conjugated secondary

antibody (Jackson Immuno Research Laboratories Inc, 1:1000 in 2% TNB) for 1 h at room temperature. Visualization of the primary antibody was performed using the Vectastain ABC kit (Vector Laboratories) and Tyramide Signal Amplification (TSA) Plus Cyanine 3 kit (PerkinElmer, 1:50 in diluent buffer). Slides were washed again and then Prolong Gold Antifade mountant with DAPI (Life technologies) was applied.

For determination of the cross-sectional area of myofibers, a serial 10 μm section of each biopsy was analyzed. To do this, sections were fixed in 4% PFA for 10 min, washed with 1x PBS and blocked with 3% BSA in 1x PBS for 60 min at room temperature. Sections were incubated overnight at 4°C with rabbit anti-laminin antibody (Sigma-Aldrich, 1:250) diluted in 1% BSA in 1x PBS. Slides were washed with 1x PBS and secondary antibody Alexa 488 goat anti-rabbit was applied for 1 h at room temperature (Life Technologies, 1:500). Slides were washed and then mounted with Prolong Gold Anti-fade mountant media (Life Technologies).

Image Processing and Analysis

All images were processed and analyzed in a blinded manner with samples being de-identified as to treatment or group. Mouse muscle samples were examined and imaged using a Leica DM5500B microscope (Leica Microsystems) at 5x-20x magnification. Images were stitched using the automated tile-scan tool to construct an image of the entire cross-section of the TA muscle. Muscle cross-sectional area (CSA) in millimeters squared was measured by tracing the muscle section border, stained with laminin, in ImageJ. Satellite cells were identified by DAPI+ and Pax7+ cell residing along the myofiber border. Myonuclei undergoing apoptosis were identified as DAPI+ and TUNEL+ cells that were within the myofiber. Satellite cells undergoing apoptosis were identified as Pax7+, TUNEL+ and DAPI+ residing along the myofiber border. DAPI+ Pax7+ TUNEL+ cells were normalized to muscle cross-sectional area and percent of cells in each cross-section relative to total number of myofibers. For transplantation experiments, donor cells were quantified by counting RFP+ (Red) fibers using the ImageJ software package (NIH, Bethesda, MD, USA).

Human muscle samples were examined and imaged using a Zeiss LSM 700 confocal microscope (Carl Zeiss MicroImaging, Jena, Germany) at 10x magnification. Images were stitched using ImageJ software package. The number and cross-sectional area of myofibers per muscle were counted and measured using laminin staining to delineate each myofiber border in serial sections. Satellite cells were identified as DAPI+ and Pax7+ cell residing along the myofiber border. The percent of Pax7+ cells are expressed relative to myofibers counted in each biopsy.

RNA-seq Preparation

RNA from freshly FACS-isolated satellite cells (70,000 – 200,000 satellite cells per mouse) was isolated using direct-Zol MicroPrep kit (R2061, Zymo Research, Irvine, CA). On-column DNase digestion was performed according to manufacturer protocols to prevent genomic DNA contamination. Total RNA was quantified using a fluorimetric RiboGreen assay. RNA and library preparation integrity were verified using a 2100 BioAnalyzer system (Agilent, Wokingham, UK), generating an RNA integrity number (RIN). All samples were at least 250 pg total RNA and RIN values of 3. Libraries were prepared using the Smarter Stranded Total RNA_Seq Kit (Clontech, Mountain View, CA, USA) following the pico input protocol using n = 3 for biological replicates. In summary, between 250 pg – 10 ng of total RNA was fragmented and then reverse transcribed into cDNA using random primers. The Template Switching Oligo was incorporated during cDNA synthesis and allowed for full length cDNA synthesis and strand specificity to be retained. Illumina sequencing adapters and barcodes were then added to the cDNA via limited PCR amplification. Next, mammalian ribosomal cDNA was enzymatically cleaved. Uncleaved fragments were PCR enriched 12-16 cycles. Final library size distribution was validated using capillary electrophoresis and quantified using fluorimetry (PicoGreen). Indexed libraries were then normalized and pooled for sequencing. Illumina libraries were hybridized to a paired end flow cell and individual fragments were clonally amplified by bridge amplification on the Illumina cBot (Illumina, Saffron Walden, UK). Once clustering was complete, the flow cell was loaded on the HiSeq 2500 and sequenced using Illumina's SBS chemistry. Upon completion of read 1, an 8 base pair index read for Index 1 was performed. The Index 1 product was then removed and the template re-anneals to the flow cell surface. The run proceeds with 7 chemistry-only cycles, followed by an 8 base pair index read to read Index 2. Finally, the library fragments were resynthesized in the reverse direction and sequenced from the opposite end of the read 1 fragment thus producing the template for paired end read 2. Base call (.bcl) files for each cycle of sequencing are generated by Illumina Real Time Analysis software. The base call files and run folders are then exported to servers maintained at the Minnesota Supercomputing Institute. Primary analysis and de-multiplexing are performed using Illumina's CASAVA software 1.8.2.

RNA-seq analysis

RNA-seq reads were aligned to *Mus musculus* reference transcriptome (GRCm38/mm10) using Kallisto (v0.44.0) quant (Bray et al., 2016), and the R package tximport (v1.10.0) was used to convert the output to Transcript Per Million (TPM) values (Soneson et al., 2015). Genes with a threshold of TPM > 5 were considered to be appreciably expressed with high confidence and used for further analysis. Principal component analysis (PCA) and hierarchical clustering were performed on 300 genes (around 10% of genes TPM > 5) with the highest variance in TPM value across all samples, using ClustVis software with default settings (Metsalu and Vilo, 2015). To identify molecular and celluar functions in which appreciably expressing genes were enriched, downstream function enrichment analysis was conducted with Ingenuity Pathway Analysis software (IPA; Ingenuity Systems, Redwood City, CA). Heatmap of differentially expressed (scERαWT versus scERαKO, fold change > 2, $p < 0.05$) and apoptosis-associated genes was generated using the R package heatmap (v1.0.12).

qRT-PCR

RNA from freshly FACS-isolated satellite cells was isolated using direct-Zol MicroPrep kit according to manufacturer's instructions. cDNA was synthesized from 10 ng RNA according to directions in SUPERVILO cDNA Synthesis Kit (11756050, ThermoFisher, Waltham, MA). Relative quantitation of the ERα (*Esr1)*, *p53*, *p38*, Beclin-1 (*Becn1*) caspase-3 (*Casp3*), *H19,* 24-Dehydrocholesterol reductase (*DhCR24*), SMAC (*DIABLO*), *and TNF* transcripts were determined using TaqMan probes (ThermoFisher) for ESR1 (Mm00433149_m1), Trp53 (Mm01731290_g1), Mapk14 (Mm01301009_m1), BECN1 (Mm00477631_m1), CASP3 (Mm01195085_m1), H19 (Mm01156721_g1), DhCR24 (Mm00519071_m1), DIABLO (Mm01194441_m1), TNF (Mm00443258_m1), and house-keeping gene gapdh (Mm99999915_g1).

Statistical Analysis

Data are presented as means ± SE. Two-way analysis of variance (ANOVA) were used to determine differences among time and treatment. Significant main effects of two-way ANOVA are indicated above the bars in the figure. If an interaction was significant, Holm-Sidak post hoc tests were used. Other mouse data were analyzed with independent *t*- tests for determining differences between groups. Human data were analyzed with Wilcoxon Signed Rank test and independent *t*- tests to determine differences between peri- and post-menopause. Analyses were conducted using SigmaPlot (version 12.5, Systat Software, Inc) for mouse data and using SPSS (version 24, IBM Corporation) for human data.

DATA AND CODE AVAILABILITY

The accession numbers for the RNA-seq data reported in this paper are shown in the Key Resources table (GEO: GSE126872 ; https://www.ncbi.nlm.nih.gov/geo/query/acc.cgi?acc=GSE126872)